Nuclear effects on tau lepton polarization in charged current deep inelastic $\nu_\tau/\bar{\nu}_\tau - A$ scattering

F. Zaidi, M. Sajjad Athar,* and S. K. Singh
Department of Physics, Aligarh Muslim University, Aligarh—202002, India

(Received 24 July 2023; accepted 7 September 2023; published 3 October 2023)

We have studied the tau-lepton polarization in the charged current $\nu_\tau/\bar{\nu}_\tau$-induced deep inelastic scattering (DIS) from the free nucleon, as well as off the nuclear targets that are being used in ongoing and proposed experiments such as IceCube, DUNE, etc. For the free nucleon target, the differential scattering cross sections are obtained by taking into account the nonperturbative effects, like target mass corrections (TMC), and the perturbative effects, like the evolution of the parton densities at the next-to-leading order (NLO) in the four-flavor $\overline{\text{MS}}$ scheme. In the case of nucleons bound inside a nuclear target, we have incorporated the nuclear medium effects such as Fermi motion, binding energy, and nucleon correlations, through the use of the nucleon spectral function. We shall present the results for the differential scattering cross sections and the longitudinal and transverse components of the tau-lepton polarization, assuming time-reversal invariance.

DOI: 10.1103/PhysRevD.108.073001

I. INTRODUCTION

In the last two decades, the particle physics community has put in appreciable efforts to study the third generation of the lepton family—i.e., the charged lepton τ^+ (τ^-) and its neutral partner $\bar{\nu}_\tau$ (ν_τ) [1,2]. Though the τ lepton was discovered for the first time in 1975 by the SLAC-LBL Collaboration [3], it took almost 25 years thereafter to detect ν_τ. The ν_τ was detected by the DONUT Collaboration [4] in 2000 based on the observation of the four ν_τ events in the charged current interaction channels. Later on, the OPERA experiment at CERN [5] observed ν_τ events in the direct appearance mode in the $\nu_\mu \to \nu_\tau$ oscillation channel. The observation of charged current ν_τ interactions is more difficult as compared to the ν_e and ν_μ interactions due to the short life of τ leptons (2.9×10^{-13} s) produced in the final state. To date, τ-lepton events with limited statistics have been observed in accelerator-based experiments such as DONUT (9 ν_τ events) [4,6], OPERA (10 ν_τ events) [5,7], and NOMAD (9 ν_τ events) [8], while 291 ν_τ candidates are reported by the atmospheric neutrino-based SuperK experiment [9], and 1806 candidates from the astrophysical sources are identified in the IceCube experiment [10,11]. So far, all the available experimental measurements have large statistical and systematic errors of about 30%–50%, which are mainly because of the low statistics and the experimental uncertainties [12]. It has been planned to study τ-lepton production with improved statistics via the decay of D_s mesons ($D_s \to \tau\nu_\tau$) in the DsTau [12] and SHiP [13] experiments, by using an emulsion detector in the FASERν [14–17] and SND@LHC [18,19] experiments, as well as through the $\nu_\mu(\bar{\nu}_\mu) \to \nu_\tau(\bar{\nu}_\tau)$ oscillation channel in the DUNE [20,21], IceCube upgrade [22,23], and T2HK [24,25] experiments that cover a wide energy spectrum of neutrinos. DUNE is the only accelerator-based experiment which has the ability to collect and accurately reconstruct the ν_τ charged current events. It is expected that at the DUNE, ν_τ events in the appearance mode would be between 100 and 1000 [20,21]. An important goal of the DUNE and HyperK experiments is to determine the neutrino mass hierarchy (normal or inverted) which relies on the ν_e flux measurements; however, it would have uncertainty arising due to $\nu_\mu(\bar{\nu}_\mu) \rightleftharpoons \nu_\tau(\bar{\nu}_\tau)$ oscillation giving rise to tauons, which decay to electrons (i.e., $\tau \to e$ decays). The study of the τ lepton and its neutral partner ν_τ is important, as it is a compelling probe to test the lepton flavor universality (LFU), which is one of the principal assumptions of the standard model of particle physics [26–28]. However, this assumption has been questioned by the observation of asymmetry measurements in the decays of B mesons into the semileptonic final states [e.g., $B^0 \to D^{*-}\tau^+\nu_\tau$; $\tau^+ \to \pi^+\pi^-\pi^+(\pi^0)\bar{\nu}_\tau$] at the LHCb experiment [29–31]. Earlier, the B meson's decay into the τ lepton has been investigated by the dedicated BABER [32,33] and Belle [34–36] experiments. The search for lepton-flavor

*Corresponding author: sajathar@gmail.com

violation may open a window to discover new physics. The upgraded Belle experiment (Belle-II), a next-generation flavor factory at the SuperKEK [37], also aims to study the τ-lepton decay modes which are relevant to test the standard model assumptions, as well as to explore the new physics beyond the SM. It is important to mention that among the charged leptons ($e^{\pm}$, $\mu^{\pm}$, $\tau^{\pm}$), the τ lepton is the only one which decays into hadrons and thus may prove to be a unique source in the study of both inclusive as well as exclusive processes, corresponding to the perturbative and nonperturbative energy regimes, respectively [38]. Furthermore, a thorough understanding of the τ-lepton properties is required for the accurate measurement of the neutrino oscillation parameters, to determine the neutrino mass hierarchy, and to reduce the existing uncertainty in the neutrino-nucleon and neutrino-nucleus scattering cross section measurements [39–42], as well as in the ν_τ observation from astrophysical sources [43–45].

Due to their heavy mass ($m_\tau = 1.78$ GeV), τ leptons produced in the charged current ν_τ interactions through various reaction channels like the quasielastic, the inelastic, and the deep inelastic scattering, are not fully polarized in the energy region of a few GeV ($E_{\nu_\tau} \lesssim 10$ GeV). It is difficult to study the reaction $\nu_\tau(\bar{\nu}_\tau) + {}^{A}_{Z}X \to \tau^{-}(\tau^{+}) + Y$ via direct detection mode due to its short lifetime, and the τ lepton is identified by the observation of its decay products such as leptons and pions, whose decay rates and topologies depend upon the production cross section and the polarization of the τ leptons. The effect of τ-lepton polarization should be studied on the τ-lepton production signal, and for estimating the background events in the $\nu_\mu \to \nu_e$ appearance channel, etc. Since the oscillation amplitude of $\nu_\mu \to \nu_\tau$ is larger than $\nu_\mu \to \nu_e$, and the branching ratio of $\tau^{\pm} \to e^{\pm}X$ is relatively large, the electron production through $\nu_\mu \to \nu_\tau \to \tau \to e$ reaction can be significant and would contribute to the background events. It is important to point out that the present neutrino event generators such as GENIE [46,47], GiBBU [48,49], NuWro [50], and NEUT [51] assume the final-state τ lepton to be purely left-handed and simulate ν_τ events just like in the case of ν_e and ν_μ events, which is not appropriate to determine the genuine number of ν_τ events in the energy region of a few GeV [52]. In the literature, various studies are available for the τ-lepton polarization in ν_τ-nucleon charged current interaction through different reaction channels such as the quasielastic, the inelastic, and the deep inelastic scattering processes. For example, in the case of the charged current $\nu_\tau - N$ quasielastic scattering process, the polarization of the final-state τ lepton has been studied by various authors [53–62], while for the inelastic processes it is discussed by some of these authors in Refs. [53–56,59,63].

The τ-lepton polarization for the deep inelastic ν_τ $(\bar{\nu}_\tau)$ scattering off the free nucleon target has been discussed in Refs. [53–56,64–66]. However, the results reported for the τ-lepton production cross sections and their polarization observables suffer from some uncertainties arising due to *(i)* the adopted choice of different limits for the kinematic constraints on W and Q^2 to demarcate the onset of DIS, and *(ii)* the use of different parametrizations of the nucleon structure functions. For example, in Refs. [53,54], authors have evaluated the DIS cross sections and the degree of polarization at NLO by directly using the PDFs grids of MRST parametrization [67]—i.e., without considering Q^2 evolution of the parton densities from the leading order (LO) to next-to-leading order (NLO). These authors also put constraints on the four-momentum transfer square, such that the nucleon structure functions are evaluated at a fixed value of $Q^2 = Q_0^2 = 1.25$ GeV^2 for all $Q^2 < Q_0^2$. Graczyk [65] uses GRV98 PDF parametrization [68] and freezes $Q^2 = Q_0^2 = 0.8$ GeV^2, without and with the Bodek-Yang corrections [69], to study the cross sections and polarization of the produced τ lepton in the $\nu_\tau - N$ scattering. Moreover, in many studies, different values of the kinematical cut on the center-of-mass (c.m.) energy (W) to define the onset of the DIS process are taken into consideration—for example, $W \geq 1.4$ GeV is taken by Hagiwara *et al.* [53] and $W \geq M + m_\pi$ is taken by Graczyk [65], while the most widely used neutrino Monte Carlo event generators like GENIE [47] and NEUT [51] take $W \geq 1.7$ GeV and $W \geq 2$ GeV, respectively. In the MINERvA experiment at the Fermilab [70], which covers a wide energy spectrum and performs EMC-like [71] measurements to study the nuclear medium modifications in (anti)neutrino-induced DIS processes off different nuclear targets, the kinematic region of $W \geq 2$ GeV and $Q^2 \geq 1$ GeV^2 is considered to be the region of true DIS events [70,72].

Since most of the neutrino experiments are performed using medium or heavy nuclear targets, a better understanding of the nuclear medium effects is crucial, especially in the low- and intermediate-energy regions. Therefore, it is also important to study the impact of the nuclear medium effects on the polarization observables of the final-state τ lepton, which may provide a complementary way to test the nuclear models available for the scattering cross sections. In the literature, the nuclear medium effects in the τ-lepton polarization for the quasielastic scattering process are discussed in various studies by Graczyk [73], Valverde *et al.* [74], Lagoda *et al.* [75], Amaro *et al.* [76], Sobczyk *et al.* [77], Hernandez *et al.* [78], Isaacson *et al.* [52], etc., while there is hardly any work, where τ-lepton polarization effects have been analyzed in $\nu_\tau(\bar{\nu}_\tau)$-induced inelastic and deep inelastic scattering processes on nuclear targets with nuclear medium effects.

In this work, for the first time, the effects of the nuclear medium have been explicitly taken into account in the study of the τ-lepton polarization in the charged-current-induced ν_τ $(\bar{\nu}_\tau)$ deep inelastic scattering on nuclear targets. Since the energy and angular distributions of the τ-lepton decay products are sensitive to the polarization of the

produced τ particles, we have studied in detail the nonvanishing components of the τ-lepton polarization and the effect of the nuclear medium on these components. Assuming time-reversal invariance, only the longitudinal (P_L) and transverse (P_T) components of polarization are nonvanishing, and the component perpendicular to the reaction plane (P_P) vanishes. The nuclear medium effects on the polarization components P_L and P_T have been studied using the methods applied earlier to study the nuclear medium effects in the calculations of differential and total cross sections in the DIS processes induced by ν_μ ($\bar{\nu}_\mu$) and ν_τ ($\bar{\nu}_\tau$) on various nuclei [42,79–82]. All the numerical calculations for scattering cross sections and polarization components are performed by considering the kinematic limits of $W \geq 2$ GeV and $Q^2 \geq 1$ GeV^2, which at present are generally taken to be the limits of the true DIS region [83]. The concerned energy region is also sensitive to the promising DUNE experiment, which is expected to observe significant ν_τ events. The liquid argon time projection chamber [21] has been recently considered to be the most promising detector to observe neutrino events; therefore, we have performed the present calculations for the ^{40}Ar nucleus, treating it to be an isoscalar nuclear target. The scattering cross section and the polarization observables P_L and P_T are expressed in terms of the nuclear structure functions $F_{iA}(x, Q^2)$; $(i = 1\text{–}5)$. These nuclear structure functions are a convolution of the nucleon spectral function and the nucleon structure functions $F_{iN}(x, Q^2)$; $(i = 1\text{–}5)$. Various perturbative and nonperturbative effects which modify the nucleon structure functions are taken into account in the different regions of x and Q^2. The special features of this work are

(1) The nucleon structure functions are calculated at NLO, and the Q^2 evolution of parton densities is performed by using the formalism developed in Refs. [41,84] in calculating the structure functions beyond the leading order.
(2) TMC in evaluating the nucleon structure functions has been taken into account following the works of Kretzer *et al.* [85].
(3) These nucleon structure functions have been used to calculate the nuclear structure functions.
(4) The effects of the nuclear medium have been studied in a microscopic field theoretical model that uses relativistic nucleon spectral functions incorporating the effects of Fermi motion, binding energy, and nucleon correlations [86]. The nucleon spectral function describes the energy and momentum distribution of the nucleons in the nucleus and is obtained by using the Lehmann representation for the relativistic nucleon propagator, and nuclear many-body theory is used to calculate it for an interacting Fermi sea in the nuclear medium [86,87]. The numerical calculations are performed in the local density approximation, where density is a function of the point of the interaction $\vec{r}$ for a given volume element.

In Sec. II, we present the formalism for the unpolarized and polarized τ lepton in the charged current $\nu_\tau/\bar{\nu}_\tau$-induced DIS processes off the free nucleon (N) and the nuclear (A) targets. In Sec. III, the results are presented, followed by discussions and conclusions.

II. FORMALISM

A. $\nu_\tau - N$ DIS: Unpolarized τ lepton

The charged current $\nu_\tau/\bar{\nu}_\tau - N$ deep inelastic scattering process depicted in Fig. 1 is

$$\nu_\tau/\bar{\nu}_\tau(k) + N(p) \to \tau^-/\tau^+(k') + X(p'), \tag{1}$$

where inside the parenthesis, the four-momenta of the corresponding particles are written. In the laboratory frame, where the target nucleon is at rest, the four-momenta are written as

$$\begin{aligned} k^\mu &= (k^0, \vec{k}) = (E_{\nu_\tau}, 0, 0, E_{\nu_\tau}), \\ k'^\mu &= (k'^0, \vec{k}') = (E_\tau, |\vec{k}'| \sin\theta, 0, |\vec{k}'| \cos\theta), \\ p^\mu &= (p^0, \vec{p}) = (M_N, 0, 0, 0), \end{aligned}$$

where $|\vec{k}'| = \sqrt{E_\tau^2 - m_\tau^2}$, and m_τ is the outgoing τ lepton mass. The expression of the differential scattering cross section for the unpolarized τ-lepton production is given by [88]

$$\frac{d^2\sigma_N}{dE_\tau d\cos\theta} = \frac{G_F^2 |\vec{k}'|}{2\pi E_{\nu_\tau} (1 + \frac{Q^2}{M_W^2})^2} L_{\mu\nu} W_N^{\mu\nu}, \tag{2}$$

with four-momentum transfer square $Q^2 = -q^2 = (k - k')^2$. G_F is the Fermi coupling constant, and M_W is the mass of the intermediate vector W boson. $W_N^{\mu\nu}$ is the nucleon hadronic tensor given by [41]

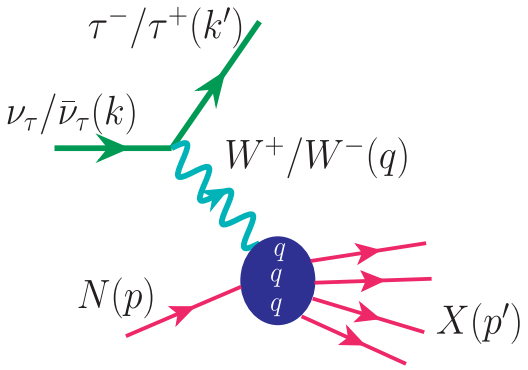

FIG. 1. Feynman diagram for the $\nu_\tau/\bar{\nu}_\tau$-induced DIS process off a free nucleon target (N).

$$W_N^{\mu\nu} = -g^{\mu\nu} W_{1N}(\nu, Q^2) + \frac{p^\mu p^\nu}{M_N^2} W_{2N}(\nu, Q^2) - \frac{i}{M_N^2} \epsilon^{\mu\nu\rho\sigma} p_\rho q_\sigma W_{3N}(\nu, Q^2) + \frac{q^\mu q^\nu}{M_N^2} W_{4N}(\nu, Q^2) + \frac{(p^\mu q^\nu + q^\mu p^\nu)}{M_N^2} W_{5N}(\nu, Q^2) + \frac{i(p^\mu q^\nu - q^\mu p^\nu)}{M_N^2} W_{6N}(\nu, Q^2), \tag{3}$$

and the unpolarized leptonic tensor $L_{\mu\nu}$ is given by [41]

$$L_{\mu\nu} = 8(k_\mu k'_\nu + k_\nu k'_\mu - k \cdot k' g_{\mu\nu} \pm i\epsilon_{\mu\nu\rho\sigma} k^\rho k'^\sigma), \tag{4}$$

where the "+" sign is for antineutrinos and the "−" sign is for neutrinos. Using Eqs. (3) and (4) in Eq. (2), we obtain the following expression of the unpolarized double differential scattering cross section:

$$\frac{d^2\sigma_N}{dE_\tau d\cos\theta} = \frac{G_F^2 |\vec{k}'|}{2\pi(1 + \frac{Q^2}{M_W^2})^2} \Big[2W_{1N}(\nu, Q^2)(E_\tau - |\vec{k}'| \cos\theta) + W_{2N}(\nu, Q^2)(E_\tau + |\vec{k}'| \cos\theta) \pm W_{3N}(\nu, Q^2) \frac{2}{M_N} (|\vec{k}'|^2 + E_{\nu_\tau} E_\tau - (E_{\nu_\tau} + E_\tau)|\vec{k}'| \cos\theta) + W_{4N}(\nu, Q^2) \frac{m_\tau^2}{M_N^2} (E_\tau - |\vec{k}'| \cos\theta) - W_{5N}(\nu, Q^2) \frac{2m_\tau^2}{M_N} \Big], \tag{5}$$

with the upper sign for neutrinos and the lower sign for antineutrinos. The contribution of the term with $W_{6N}(\nu, Q^2)$ vanishes when contracted with the leptonic tensor $L_{\mu\nu}$. When Q^2 and ν become large, the structure functions $W_{iN}(\nu, Q^2)$; $(i = 1\text{–}5)$ are generally expressed in terms of the dimensionless nucleon structure functions $F_{iN}(x)$, $i = 1\text{–}5$ as

$$F_{1N}(x) = W_{1N}(\nu, Q^2); \qquad F_{2N}(x) = \frac{Q^2}{2xM_N^2} W_{2N}(\nu, Q^2);$$
$$F_{3N}(x) = \frac{Q^2}{xM_N^2} W_{3N}(\nu, Q^2), \tag{6}$$

$$F_{4N}(x) = \frac{Q^2}{2M_N^2} W_{4N}(\nu, Q^2); \quad F_{5N}(x) = \frac{Q^2}{2xM_N^2} W_{5N}(\nu, Q^2). \tag{7}$$

We observe that the scattering cross section [Eq. (5)] obtained using the aforementioned relations does not satisfy the positivity condition in the neighborhood of the threshold region. Therefore, we made the following modification in the $F_{1N}(x)$ structure function in order to ensure the positivity constraints as a result of which the allowed kinematic region for the τ-lepton polarization gets reduced [53,66]:

$$F_{1N}(x) = \frac{W_{1N}(\nu, Q^2)}{(1 + \frac{xM_N}{\nu})}. \tag{8}$$

In the above expressions, $x(= \frac{Q^2}{2p\cdot q})$ is the Bjorken scaling variable which lies in the range of $\frac{m_\tau^2}{2M_N(E_{\nu_\tau} - m_\tau)} \leq x \leq 1$, and $\nu = yE_{\nu_\tau} = E_{\nu_\tau} - E_\tau$ is the energy transfer. In Fig. 2, we have shown the allowed kinematic region in the "$|\vec{k}'| \cos\theta$"-"$|\vec{k}'| \sin\theta$" plane (left panel), the "Bjorken x"-"inelasticity y" plane (middle panel), and the "W"-"Q^2" plane (right panel), at $E_{\nu_\tau} = 10$ GeV. It may be noticed that the kinematic region with a $W \geq 2$ GeV cut is much suppressed as compared to the case when a cut of $W \geq 1.4$ GeV is applied. The existing ambiguity in the choice of center-of-mass energy cut in the literature needs more attention from the particle physics community and has been recently discussed in Ref. [83]. We have considered the region of $Q^2 \geq 1$ GeV^2 and $W \geq 2$ GeV to be the region of true DIS events and apply these constrains in the numerical calculations. It must be noticed that for the true DIS events, we could not dig out the information from the regions of low as well as high values of x and y; only the intermediate region of scaling variables $[0.2 \leq (x, y) < 0.8]$ is accessible at the chosen value of ν_τ energies in the present work.

Using the relations given in Eqs. (6) and (7) in Eq. (5), we obtain the differential scattering cross section in terms of the dimensionless nucleon structure functions:

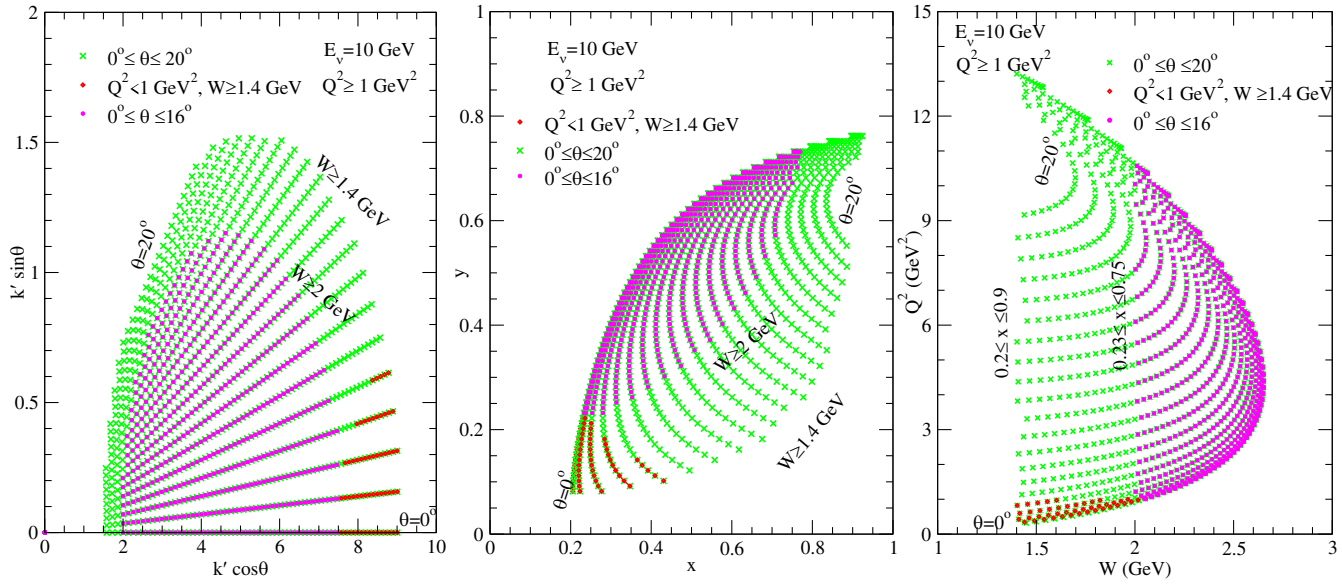

FIG. 2. Kinematically allowed region for the $\nu_\tau - N$ induced DIS process at $E_{\nu_\tau} = 10$ GeV with different constraints on center-of-mass energy W—i.e., $W \geq 1.4$ GeV and $W \geq 2$ GeV. Diamond-shaped points correspond to the region where $Q^2 < 1$ GeV^2.

$$\frac{d^2\sigma_N}{dE_\tau d\cos\theta} = \frac{G_F^2|\vec{k}'|}{2\pi M_N(1+\frac{Q^2}{M_W^2})^2}\left[2F_{1N}(x,Q^2)(E_\tau - |\vec{k}'|\cos\theta) + F_{2N}(x,Q^2)\frac{M_N}{\nu}(E_\tau + |\vec{k}'|\cos\theta)\right.$$
$$\pm F_{3N}(x,Q^2)\frac{1}{\nu}(|\vec{k}'|^2 + E_{\nu_\tau}E_\tau - (E_{\nu_\tau}+E_\tau)|\vec{k}'|\cos\theta) + F_{4N}(x,Q^2)\frac{m_\tau^2}{\nu M_N x}(E_\tau - |\vec{k}'|\cos\theta)$$
$$\left. - F_{5N}(x,Q^2)\frac{2m_\tau^2}{\nu}\right]. \tag{9}$$

The dimensionless nucleon structure functions are written in terms of the parton distribution functions $q_i(x)$ and $\bar{q}_i(x)$ at the leading order as

$$F_{2N}(x) = \sum_i x[q_i(x) + \bar{q}_i(x)]; \qquad xF_{3N}(x) = \sum_i x[q_i(x) - \bar{q}_i(x)]; \qquad F_{4N}(x) = 0. \tag{10}$$

For an isoscalar nucleon target, $F_{2N}(x)$ and $F_{3N}(x)$ in the four-flavor scheme are given by

$$F_{2N}^{\nu_\tau}(x) = x[u(x)+d(x)+\bar{u}(x)+\bar{d}(x)+2s(x)+2\bar{c}(x)], \quad F_{2N}^{\bar{\nu}_\tau}(x) = x[u(x)+d(x)+\bar{u}(x)+\bar{d}(x)+2\bar{s}(x)+2c(x)],$$
$$xF_{3N}^{\nu_\tau}(x) = x[u(x)+d(x)-\bar{u}(x)-\bar{d}(x)+2s(x)-2\bar{c}(x)], \quad xF_{3N}^{\bar{\nu}_\tau}(x) = x[u(x)+d(x)-\bar{u}(x)-\bar{d}(x)-2\bar{s}(x)+2c(x)].$$

We have treated all the four flavors of quarks to be massless, as we have found that the effect of the massive charm quark is very small in the present kinematic region. These details have already been discussed in Refs. [41,42]. To define the structure functions $F_{1N}(x)$ and $F_{5N}(x)$ at the leading order, we use Callan-Gross [89] and Albright-Jarlskog [64] relations, respectively, as

$$F_{1N}(x) = \frac{F_{2N}(x)}{2x}; \qquad F_{5N}(x) = \frac{F_{2N}(x)}{2x}.$$

As the kinematic region of the low and moderate Q^2, the region of our particular interest is sensitive to the perturbative and nonperturbative QCD corrections, such as the evolution of parton densities beyond the leading order and the TMC effect, respectively; these effects have been taken into account while evaluating the nucleon structure functions [41]. We have used the Martin-Motylinski-Harland-Lang-Thorne (MMHT) parton distribution functions (PDFs) parametrization [90] up to NLO in the four-flavor (u, d, s, and c) minimal subtraction (MSbar)

scheme. Furthermore, target mass correction effect has been incorporated following Refs. [41,85].

For the polarized tau lepton, the hadronic current remains the same, while the leptonic current gets modified (see Fig. 1). In the next section, we present the formalism for the production of polarized τ leptons in the charged-current-induced $\nu_\tau/\bar{\nu}_\tau - N$ DIS processes.

B. $\nu_\tau - N$ DIS: Polarized τ lepton

In the case of a polarized $\tau^{\mp}$ lepton (as depicted in Fig. 3), the leptonic tensor modifies to [77]

$$L_{\mu\nu}(s;h) = \frac{1}{2}[L_{\mu\nu} \mp h m_\tau s^\alpha (k_\mu g_{\nu\alpha} + k_\nu g_{\mu\alpha} - k_\alpha g_{\mu\nu} \pm i\epsilon_{\mu\nu\alpha\beta}k^\beta)], \tag{11}$$

where $h = \pm 1$ is the helicity, s^α is the spin four-vector, the upper sign is for neutrinos, and the lower sign is for antineutrinos. We choose the axis of quantization specified by the unit vector $\hat{n}$ in the rest frame of the τ lepton $[k'^\mu = (k'^0, \vec{0})]$ and define s^α in this frame as follows:

$$s^\alpha = (0, \hat{n}). \tag{12}$$

However, in any other frame, it is given by [77]

$$s^\alpha = \left(\frac{\vec{k}' \cdot \hat{n}}{m_\tau}, \hat{n} + \frac{\vec{k}'}{m_\tau}\frac{(\vec{k}' \cdot \hat{n})}{(E_\tau + m_\tau)}\right), \tag{13}$$

following the scalar product invariance and ensuring that $s^2 = -1$ and $s \cdot k' = 0$. Using these expressions, we have obtained the polarized double differential scattering cross section as

$$\frac{d^2\sigma_N^{\rm pol}}{dE_\tau d\cos\theta} = \frac{G_F^2 |\vec{k}'|}{2\pi E_{\nu_\tau}(1 + \frac{Q^2}{M_W^2})^2} L_{\mu\nu}(s;h) W_N^{\mu\nu}. \tag{14}$$

After contracting the polarized leptonic tensor given in Eq. (11) with the hadronic tensor [Eq. (3)], we get [77,78]

$$\frac{d^2\sigma_N^{\rm pol}}{dE_\tau d\cos\theta} = (1 \pm h s^\alpha \mathcal{P}^\alpha)\frac{d^2\sigma_N}{dE_\tau d\cos\theta}, \tag{15}$$

where the upper sign stands for neutrinos, the lower sign is for the antineutrino-induced processes, and $\mathcal{P}^\alpha$ is the polarization vector of the final-state charged lepton that is obtained by taking the nucleon response [77,78]:

$$\mathcal{P}^\alpha = \mp \frac{m_\tau (k_\mu g_{\nu\alpha} + k_\nu g_{\mu\alpha} - k_\alpha g_{\mu\nu} \pm i\epsilon_{\mu\nu\alpha\beta}k^\beta) W_N^{\mu\nu}}{L_{\mu\nu} W_N^{\mu\nu}}. \tag{16}$$

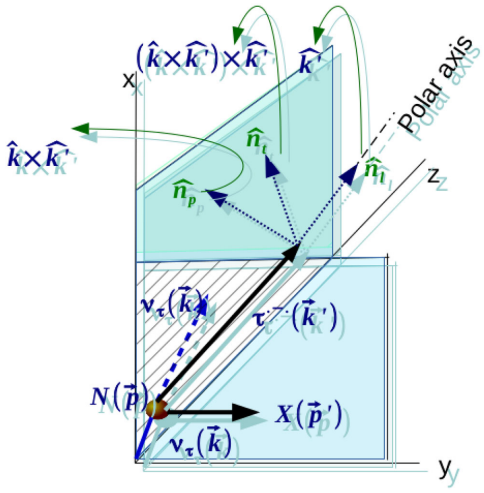

FIG. 3. Momentum and polarization directions of the produced τ lepton. The orthogonal unit vectors $\hat{n}_l$, $\hat{n}_t$, and $\hat{n}_p$ correspond to the longitudinal, transverse, and perpendicular directions, respectively, with respect to the τ-lepton momentum.

The polarization vector is decomposed into longitudinal (in the direction to the outgoing τ-lepton momentum $\vec{k}'$), perpendicular (in the orthogonal direction to the $\nu_\tau - \tau$ plane) and transverse (transverse to $\vec{k}'$ and in the $\nu_\tau - \tau$ plane) components as

$$\mathcal{P}^\alpha = -(\underbrace{P_L n_l^\alpha}_{\text{longitudinal}} + \underbrace{P_T n_t^\alpha}_{\text{transverse}} + \underbrace{P_P n_p^\alpha}_{\text{perpendicular}}), \tag{17}$$

where $n_i^\alpha; (i = l, t, p)$ are the orthogonal basis of the four-vector Minkowski space, and are defined as

$$n_l^\alpha = \left(\frac{|\vec{k}'|}{m_\tau}, \frac{E_\tau \vec{k}'}{m_\tau |\vec{k}'|}\right), \qquad n_t^\alpha = \left(0, \frac{(\vec{k}\times\vec{k}')\times\vec{k}'}{|(\vec{k}\times\vec{k}')\times\vec{k}'|}\right),$$
$$n_p^\alpha = \left(0, \frac{\vec{k}\times\vec{k}'}{|\vec{k}\times\vec{k}'|}\right). \tag{18}$$

Thus, the different polarization components are obtained as

$$P_L = -\mathcal{P}^\alpha \cdot n_l^\alpha, \quad P_T = -\mathcal{P}^\alpha \cdot n_t^\alpha, \quad P_P = -\mathcal{P}^\alpha \cdot n_p^\alpha. \tag{19}$$

We find that $\mathcal{P}^\alpha \cdot n_p^\alpha = 0$, which implies that the perpendicular component (P_P) does not contribute, as the polarization three-vector lies in the direction perpendicular to the τ-lepton scattering plane. However, on simplification of the above expression in the laboratory frame, we obtain [53,78]

$$P_L = \mp \frac{E_{\nu_\tau}}{L_{\mu\nu} W_N^{\mu\nu}} \left[\left(2F_{1N}(x,Q^2) - \frac{m_\tau^2}{M_N \nu x} F_{4N}(x,Q^2) \right) (|\vec{k}'| - E_\tau \cos\theta) + F_{2N}(x,Q^2) \frac{M_N}{\nu} (|\vec{k}'| + E_\tau \cos\theta) \right.$$
$$\left. \pm \frac{F_{3N}(x,Q^2)}{\nu} (|\vec{k}'|(E_{\nu_\tau} + E_\tau) - (|\vec{k}'|^2 + E_{\nu_\tau} E_\tau) \cos\theta) - \frac{2}{\nu} m_\tau^2 \cos\theta F_{5N}(x,Q^2) \right], \quad (20)$$

$$P_T = \mp \frac{m_\tau \sin\theta E_{\nu_\tau}}{L_{\mu\nu} W_N^{\mu\nu}} \left[2F_{1N}(x,Q^2) - F_{2N}(x,Q^2) \frac{M_N}{\nu} \pm \frac{E_{\nu_\tau}}{\nu} F_{3N}(x,Q^2) - \frac{m_\tau^2}{M_N \nu x} F_{4N}(x,Q^2) + \frac{2E_\tau}{\nu} F_{5N}(x,Q^2) \right], \quad (21)$$

where the upper sign corresponds to the case of neutrinos and the lower sign corresponds to the antineutrino case. It may be noticed that the polarization components depend upon the lepton kinematic variables—i.e., the lepton energy E_τ and scattering angle θ—as well as upon the dimensionless nucleon structure functions, $F_{iN}(x,Q^2)$; $(i = 1\text{–}5)$, and thus exhibit the particular sensitivities to the different elements used in the scattering cross section models. The degree of polarization P, a Lorentz-invariant quantity, is given by [53]

$$P^2 = (P_L^2 + P_T^2) \Rightarrow P = \sqrt{P_L^2 + P_T^2} \leq 1. \quad (22)$$

For a fully polarized τ lepton, $P = 1$, while in the case of the partially polarized τ lepton, the degree of polarization lies in the range of $0 < P < 1$, and for the unpolarized τ lepton, the degree of polarization is zero. To specify the direction of polarization, we define the spin polarization vector in the rest frame of the τ lepton as [53]

$$\vec{s} = (s_x, s_y, s_z) = P(\sin\theta_P \cos\phi_P, \sin\theta_P \sin\phi_P, \cos\theta_P), \quad (23)$$

where the z axis is taken along the direction of tauon momentum, θ_P is the polar angle, and ϕ_P is the azimuthal angle of the spin polarization vector. ϕ_P may have values of either 0 or π corresponding to $\vec{k}'$, constraining that the polarization vector always remains in the scattering plane. Hence, the direction of polarization is determined by the polar component of the normalized polarization vector—i.e. [53],

$$\cos\theta_P = \frac{s_z}{P} = \frac{P_L}{P}. \quad (24)$$

C. $\nu_\tau - A$ DIS: Nuclear medium effects

The differential scattering cross section for the charged-current-inclusive $\nu_\tau/\bar{\nu}_\tau$ nucleus deep inelastic scattering process (depicted in Fig. 4),

$$\nu_\tau/\bar{\nu}_\tau(k) + A(p_A) \to \tau^-/\tau^+(k') + X(p_A'), \quad (25)$$

is given by

$$\frac{d^2\sigma_A}{dE_\tau d\cos\theta} = \frac{G_F^2 |\vec{k}'|}{2\pi E_{\nu_\tau} (1 + \frac{Q^2}{M_W^2})^2} L_{\mu\nu} W_A^{\mu\nu}, \quad (26)$$

where $W_A^{\mu\nu}$ is the nuclear hadronic tensor and is expressed in terms of the dimensionless nuclear structure functions $F_{iA}(x)$; $(i = 1\text{–}5)$ as

$$W_A^{\mu\nu} = -g^{\mu\nu} W_{1A}(\nu,Q^2) + \frac{p_A^\mu p_A^\nu}{M_N^2} W_{2A}(\nu,Q^2) - \frac{i}{M_N^2} \epsilon^{\mu\nu\rho\sigma} p_{A\rho} q_\sigma W_{3A}(\nu,Q^2) + \frac{q^\mu q^\nu}{M_N^2} W_{4A}(\nu,Q^2)$$
$$+ \frac{(p_A^\mu q^\nu + q^\mu p_A^\nu)}{M_N^2} W_{5A}(\nu,Q^2) + \frac{i(p_A^\mu q^\nu - q^\mu p_A^\nu)}{M_N^2} W_{6A}(\nu,Q^2). \quad (27)$$

Following the same analogy as that for a free nucleon target, we have obtained the following expression of the double differential scattering cross section for the nucleons bound inside a nuclear target:

$$\frac{d^2\sigma_A}{dE_\tau d\cos\theta} = \frac{G_F^2 |\vec{k}|}{2\pi M_N (1 + \frac{Q^2}{M_W^2})^2} \left[2F_{1A}(x,Q^2)(E_\tau - |\vec{k}|\cos\theta) + F_{2A}(x,Q^2) \frac{M_N}{\nu} (E_\tau + |\vec{k}|\cos\theta) \right.$$
$$\left. \pm F_{3A}(x,Q^2) \frac{1}{\nu} (|\vec{k}|^2 + E_{\nu_\tau} E_\tau - (E_{\nu_\tau} + E_\tau)|\vec{k}|\cos\theta) + F_{4A}(x,Q^2) \frac{m_\tau^2}{\nu M_N x} (E_\tau - |\vec{k}|\cos\theta) - F_{5A}(x,Q^2) \frac{2m_\tau^2}{\nu} \right]. \quad (28)$$

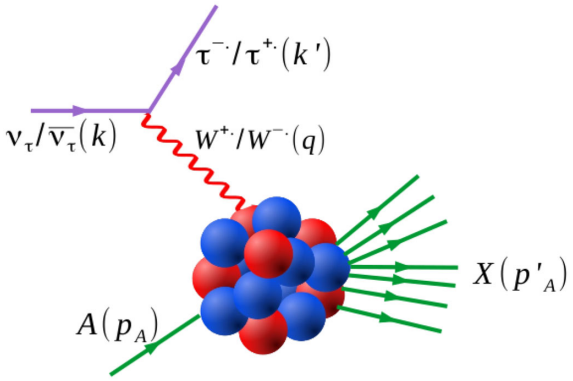

FIG. 4. Feynman diagram for the $\nu_\tau/\bar{\nu}_\tau$-induced DIS process off a nuclear target (A).

In the present work, we consider the scattering process in the laboratory frame, where the target nucleus is at rest—i.e., $p_A = (p_A^0, \vec{p}_A = 0)$—and the momentum of the nucleon ($\vec{p}_N$) in the nucleus is nonzero, and the motion of such nucleons corresponds to the Fermi motion. In the local density approximation, the lepton scatters from a bound nucleon having density $\rho_N(r)$ and the corresponding Fermi momentum $p_{F_N}(r) = (3\pi^2\rho_N(r))^{1/3}$. The local density $\rho_N(r)$ of protons or neutrons bound inside the nucleus is given by $\rho_p(r) = \frac{Z}{A}\rho(r)$ and $\rho_n(r) = \frac{A-Z}{A}\rho(r)$, where $\rho(r)$ is the nuclear density which is calculated by using the parametrization of 2pF density—i.e., $\rho(r) = \frac{\rho_0}{1+e^{(r-c_1)/c_2}}$. ρ_0 is the central density, and c_1 and c_2 are the density parameters which are determined through the electron scattering experiments [91,92]. The details can be found in Ref. [81]. The differential cross section ($d\sigma_A$) for $\nu_\tau/\bar{\nu}_\tau - A$ scattering is obtained by folding the $\nu_\tau/\bar{\nu}_\tau - N$ scattering cross section ($d\sigma_N$) with $\rho_N(r)$ and integrating over the volume element:

$$d\sigma_A = \int d^3r \rho_N(r) d\sigma_N. \tag{29}$$

In the case of symmetric nuclear matter, each nucleon occupies a volume of $(2\pi\hbar)^3$, and due to the two possible spin orientations of the nucleon, each unit cell in the configuration space is occupied by the two nucleons. Hence, the number of nucleons for a given volume ($\hbar = 1$ in natural units) is

$$N = 4V \int_0^{p_{F_N}} \frac{d^3p_N}{(2\pi)^3} n(\vec{p}_N, \vec{r}), \tag{30}$$

$$\Rightarrow \rho = \frac{N}{V} = 4 \int_0^{p_{F_N}} \frac{d^3p_N}{(2\pi)^3} n(\vec{p}_N, \vec{r}), \tag{31}$$

where $n(\vec{p}_N, \vec{r}) = \theta(p_{F_N}(\vec{r}) - |\vec{p}_N|)$ is the occupation number of the initial nucleon carrying momentum $\vec{p}_N$, and it has dependence on the radial coordinates due to the Fermi momentum $p_{F_N}(r)$. The occupation number corresponding to the nucleon within the Fermi sea fulfills the following condition:

$$n(\vec{p}_N) = \begin{cases} 1 & \text{for } \vec{p}_N \le \vec{p}_{F_N} \\ 0 & \text{for } \vec{p}_N > \vec{p}_{F_N} \end{cases}. \tag{32}$$

We have chosen the four-momentum transfer along the z axis; therefore, $q^\mu = (q^0, 0, 0, q^z)$, and the Bjorken variable x_N corresponding to the nucleon bound inside a nucleus is then expressed as

$$x_N = \frac{Q^2}{2p_N \cdot q} = \frac{Q^2}{2(p_N^0 q^0 - p_N^z q^z)}. \tag{33}$$

The Bjorken variable for the nuclear target x_A is given by

$$x_A = \frac{Q^2}{2p_A \cdot q} = \frac{Q^2}{2p_A^0 q^0} = \frac{Q^2}{2AM_N q^0} = \frac{x}{A}. \tag{34}$$

The nucleons inside a nuclear target interact among themselves via the strong interaction; hence, various nuclear medium effects come into play depending upon the value of the Bjorken variable x. Nuclear effects such as Fermi motion, binding, and nucleon correlations have been taken into account for an inclusive process by using the hole spectral function (S_h) calculated in a microscopic field theoretical model [86,87]. The hole spectral function is properly normalized and has been checked by obtaining the correct baryon number (A) and nuclear binding energy for a given nuclear target [79,93]:

$$4 \int d^3r \int \frac{d^3p_N}{(2\pi)^3} \int_{-\infty}^{\mu} S_h(\omega, \vec{p_N}, \rho(r)) d\omega = A, \tag{35}$$

where μ is the chemical potential and ω is the removal energy [87]. We have obtained the differential scattering cross section in terms of the hole spectral function as [42,81]

$$\frac{d^2\sigma_A}{dE_\tau d\cos\theta} = \frac{G_F^2 |\vec{k}'|}{2\pi E_{\nu_\tau} (1 + \frac{Q^2}{M_W^2})^2} L_{\mu\nu} 4 \int d^3r \int \frac{d^3p_N}{(2\pi)^3} \frac{M_N}{E(\vec{p}_N)} \times \int_{-\infty}^{\mu} dp_N^0 S_h(p_N^0, \vec{p}_N, \rho(r)) W_N^{\mu\nu}(p_N, q). \tag{36}$$

Comparing Eqs. (26) and (36), we obtain the nuclear hadronic tensor $W_A^{\mu\nu}$ in terms of the nucleonic tensor $W_N^{\mu\nu}$ convoluted over the hole spectral function S_h [42]:

$$W_A^{\mu\nu} = 4 \int d^3r \int \frac{d^3p_N}{(2\pi)^3} \frac{M_N}{E(\vec{p}_N)} \times \int_{-\infty}^{\mu} dp_N^0 S_h(p_N^0, \vec{p}_N, \rho(r)) W_N^{\mu\nu}(p_N, q), \tag{37}$$

where the factor of 4 is because of the spin-isospin degrees of freedom of the nucleon for an isoscalar nuclear target. We take the appropriate components of the nucleon [$W_N^{\mu\nu}$ in Eq. (3)] and the nuclear [$W_A^{\mu\nu}$ in Eq. (27)] hadronic tensors along the x, y, and z axes and obtained the expressions for the nuclear structure functions as [42]

$$F_{iA}(x_A, Q^2) = 4 \int d^3r \int \frac{d^3p_N}{(2\pi)^3} \frac{M_N}{E_N(\vec{p}_N)} \times \int_{-\infty}^{\mu} dp^0 S_h(p_N^0, \vec{p}_N, \rho(r)) \times f_{iN}(x, Q^2); \quad i = 1 - 5, \tag{38}$$

where

$$f_{1N}(x, Q^2) = AM_N \left[\frac{F_{1N}(x_N, Q^2)}{M_N} + \left(\frac{p_N^x}{M_N} \right)^2 \frac{F_{2N}(x_N, Q^2)}{\nu_N} \right], \tag{39}$$

$$f_{2N}(x, Q^2) = \left(\frac{F_{2N}(x_N, Q^2)}{M_N^2 \nu_N} \right) \times \left[\frac{Q^4}{q^0 (q^z)^2} \left(p_N^z + \frac{q^0 (p_N^0 - \gamma p_N^z)}{Q^2} q^z \right)^2 + \frac{q^0 Q^2 (p_N^x)^2}{(q^z)^2} \right], \tag{40}$$

$$f_{3N}(x, Q^2) = A \frac{q^0}{q^z} \times \left(\frac{p_N^0 q^z - p_N^z q^0}{p_N \cdot q} \right) F_{3N}(x_N, Q^2), \tag{41}$$

$$f_{4N}(x, Q^2) = A \left[F_{4N}(x_N, Q^2) + \frac{p_N^z Q^2}{q^z} \frac{F_{5N}(x, Q^2)}{M_N \nu_N} \right], \tag{42}$$

$$f_{5N}(x, Q^2) = A \frac{F_{5N}(x_N, Q^2)}{M_N \nu_N} \times \left[q^0 (p_N^0 - \gamma p_N^z) + Q^2 \frac{p_N^z}{q^z} \right], \tag{43}$$

and $\gamma = \frac{q^z}{q^0}$.

The nucleons which are bound inside the nucleus interact with each other via meson exchange such as π, ρ, etc. The interaction of the intermediate vector boson (IVB) with the mesons plays an important role in the evaluation of nuclear structure functions [42,79,88,93–95]. In the low region of x, the contribution from shadowing ($0 < x < 0.1$) and antishadowing ($0.1 < x < 0.2$) effects is important. However, in the present kinematic region of x and Q^2, we have found that the mesonic contribution and the (anti) shadowing effect are almost negligible; therefore, we have not included these effects while presenting the results. It must be pointed out that in our earlier studies, we have observed the nonisoscalarity corrections in argon to be very small in the kinematic region of present interest [42,80–82].

All the numerical results are obtained in the energy range of $6 \leq E_{\nu_\tau} \leq 20$ GeV by taking into account the target mass-correction effect at the next-to-leading order in the kinematic region of $Q^2 \geq 1$ GeV^2. To understand the effect of the center-of-mass energy cut, we have obtained the results in various kinematic regions using different cuts on W—i.e., $W \geq 1.4$ GeV, $W \geq 1.6$ GeV, and $W \geq 2$ GeV.

III. DISCUSSION OF RESULTS AND CONCLUSIONS

In this section, we present the results for the τ-lepton production cross section by using Eqs. (9) and (28), as well as its polarization observables, such as the degree of polarization (P), longitudinally (P_L) and transversely (P_T) polarized components, and the direction of the polarization vector as defined through Eqs. (20)–(24).

A. Free nucleon

1. Neutrino-induced reactions

In Fig. 5, we present the numerical results for various observables in the case of the charged current ν_τ-nucleon DIS process at different values of the incoming neutrino energies, viz. $E_{\nu_\tau} = 6$, 10, and 20 GeV. In this figure, the results for the double differential scattering cross section $\frac{d^2\sigma_N}{dE_\tau d\cos\theta}$ (top panel), the degree of polarization P (middle panel), and the polar component of the normalized polarization vector $\cos\theta_P$ (bottom panel), vs the final-state charged lepton energy (E_τ), are presented at different values of lepton scattering angle θ in the laboratory frame viz. $\theta = 0°, 2.5°, 5°$ and 10°. The results presented in this figure describe the angular and energy dependence of the above observables and the impact of applying different kinematic cuts on the c.m. energy W. In the following, we present our results for each of the above observables in the case of neutrino reactions.

(1) Differential cross section:
   (a) With the increase in neutrino energy, the deep inelastic cross section spans over a wide lepton energy range but has a smaller magnitude at a given lepton energy E_τ, as compared to the results obtained at the lower neutrino energies. This result is applicable for all angles in the range of $0° \leq \theta \leq 10°$ studied in this work, but the reduction is smaller with the increase in θ. For example, at a fixed τ-lepton energy of $E_\tau =$ 4 GeV and $\theta = 2.5°$, the reduction in the cross section at $E_{\nu_\tau} = 10$ GeV is around 28% as compared to the cross section at $E_{\nu_\tau} = 6$ GeV. This reduction is observed to be 15% at $\theta = 10°$.
   (b) For a fixed neutrino energy, the τ-lepton production cross section increases with τ-lepton energy E_τ, for a given scattering angle. For example, at $E_{\nu_\tau} = 10$ GeV and scattering angle

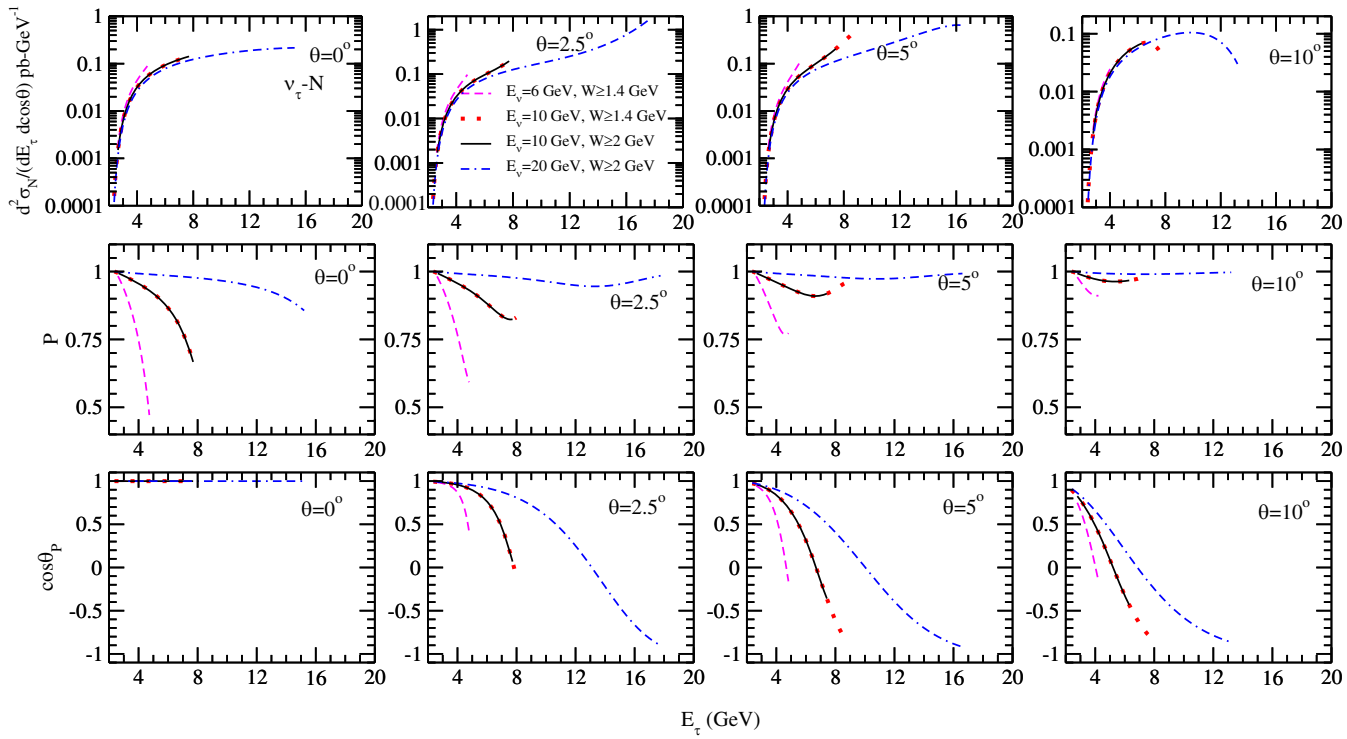

FIG. 5. *(i) Top panels:* the differential scattering cross section, *(ii) Middle panels:* the degree of polarization (P), and *(iii) Bottom panels:* the polar component of the normalized polarization vector, vs the outgoing charged lepton energy (E_τ), at the different values of incoming neutrino energy—i.e., $E_{\nu_\tau} = 6$ GeV, 10 GeV, and 20 GeV. The numerical results for $\nu_\tau - N$ are obtained with target mass correction effect at the next-to-leading order. These results are obtained for $W \geq 1.4$ GeV and $W \geq 2$ GeV cut on the center-of-mass energy.

$\theta = 5°$, the cross section increases with the τ-lepton energy by 70% when we move from $E_\tau = 4$ GeV to $E_\tau = 6$ GeV.

(c) As far as the angular dependence is concerned, for a fixed neutrino energy and for a fixed τ-lepton energy, the cross section decreases as we increase the scattering angle. For example, at $E_{\nu_\tau} = 10$ GeV and $E_\tau = 4$ GeV, there is a reduction in the cross section of about 8% as we move from $\theta = 0°$ to $\theta = 5°$.

(d) Furthermore, it may also be observed from the figure that due to the kinematical constraint on the c.m. energy, at $E_{\nu_\tau} = 10$ GeV, the τ-lepton production cross section with $W \geq 2$ GeV (solid line) gets kinematically restricted in τ-lepton energy as compared to the cross section with $W \geq 1.4$ GeV (dotted line). For example, at $\theta = 5°$, the kinematically allowed region for τ-lepton energy is $2.3 \leq E_\tau \leq 8.8$ GeV for $W \geq 1.4$ GeV, which reduces to $2.6 \leq E_\tau \leq 7.4$ GeV when a cut of $W \geq 2$ GeV is applied.

(2) Degree of polarization (P):

(a) The degree of polarization (P) of the final-state charged lepton (shown in the middle panels) deviates from unity for *(a)* the lower neutrino energies, *(b)* the higher-energy values of the produced τ lepton, and *(c)* small scattering angles, implying that the produced τ lepton is partially polarized in this kinematic region.

(b) For a given lepton energy E_τ, the degree of polarization increases with the neutrino energy E_{ν_τ}. Quantitatively, for $E_{\nu_\tau} = 10$ GeV and $\theta = 0°(5°)$, the deviation from unity is about 3% (4%) at $E_\tau = 4$ GeV; however, for $E_{\nu_\tau} = 20$ GeV, the outgoing lepton is almost polarized with a deviation of 1%–3% for all the scattering angles considered here.

(c) For a given neutrino energy E_{ν_τ}, the degree of polarization decreases with the increase in τ-lepton energy—say, at $E_{\nu_\tau} = 6$ GeV and $\theta = 0°$, the deviation of P from unity is 7% for $E_\tau = 3$ GeV and 25% for $E_\tau = 4$ GeV.

(d) For a given neutrino energy E_{ν_τ} and lepton energy E_τ, the degree of polarization increases with the lab scattering angle θ. For example, at $E_{\nu_\tau} = 6$ GeV and $E_\tau = 3$ GeV, the deviation of the degree of polarization from unity is found to be 7% for the forward-scattering angle $\theta = 0°$; however, for $\theta = 5°$, it decreases to 6% and becomes 4% for $\theta = 10°$.

(3) Polar component of normalized polarization vector ($\cos\theta_P$):
   (a) The value of the polar component of the normalized polarization vector is $\cos\theta_P = +1$ at the forward-scattering angle for the entire range of E_τ. At the nonzero values of the lepton scattering angle, θ (considered here), $\cos\theta_P$ is negative in the higher-energy range of the charged lepton (E_τ), while for the lower-energy range, the polarization vector changes its direction and $\cos\theta_P$ possesses positive values.
   (b) For a given value of E_τ and θ, $\cos\theta_P$ increases with the increase in neutrino energy, quantitatively; at $E_\tau = 4$ GeV and $\theta = 5°$, it is found to be 15% higher for $E_\nu = 10$ GeV as compared to the case of $E_\nu = 6$ GeV as shown in the figure.

We have found that the qualitative behavior of these results is similar to the results reported by Hagiwara *et al.* [53,54], Aoki *et al.* [55], and Graczyk [65]. However, quantitatively, there are some differences due to the use of different PDFs, Q^2 evolution, and the cuts of c.m. energy W.

2. Antineutrino-induced reactions

In Fig. 6, the corresponding results are shown for the $\bar{\nu}_\tau - N$ induced τ^+-lepton production processes, at the different values of E_{ν_τ} viz. 8 GeV (dashed line), 10 GeV (solid line), and 20 GeV (dash-dotted line) for the kinematical conditions similar to the case of the charged current $\nu_\tau - N$ DIS process (Fig. 5). These results are obtained by applying a cut of 2 GeV on W. These results for the antineutrino-nucleon interaction are discussed below.

(1) Differential cross section:
   The qualitative behavior of the scattering cross section is similar for both $\nu_\tau - N$ and $\bar{\nu}_\tau - N$ DIS processes, while quantitatively the τ^+-lepton production cross sections are smaller as compared to the case of τ^--lepton production. For example, at the fixed values of $E_{\nu_\tau} = 10$ GeV and $E_\tau = 6$ GeV, this suppression is found to be about 82% at $\theta = 0°$, 80% at $\theta = 2.5°$, and 70% at $\theta = 10°$.

(2) Degree of polarization (P):
   (a) The results obtained for the degree of polarization for the τ^+ lepton are different from the corresponding results for the τ^--lepton polarization. It may be noticed from the figure that at the lower values of E_τ, the outgoing τ^+ lepton possesses a good strength of the degree of polarization P. As we move toward the higher values of E_τ, the value of P gets reduced until it approaches the minimum, at which τ^+ is likely to be less polarized. However, with further increase in E_τ, the degree

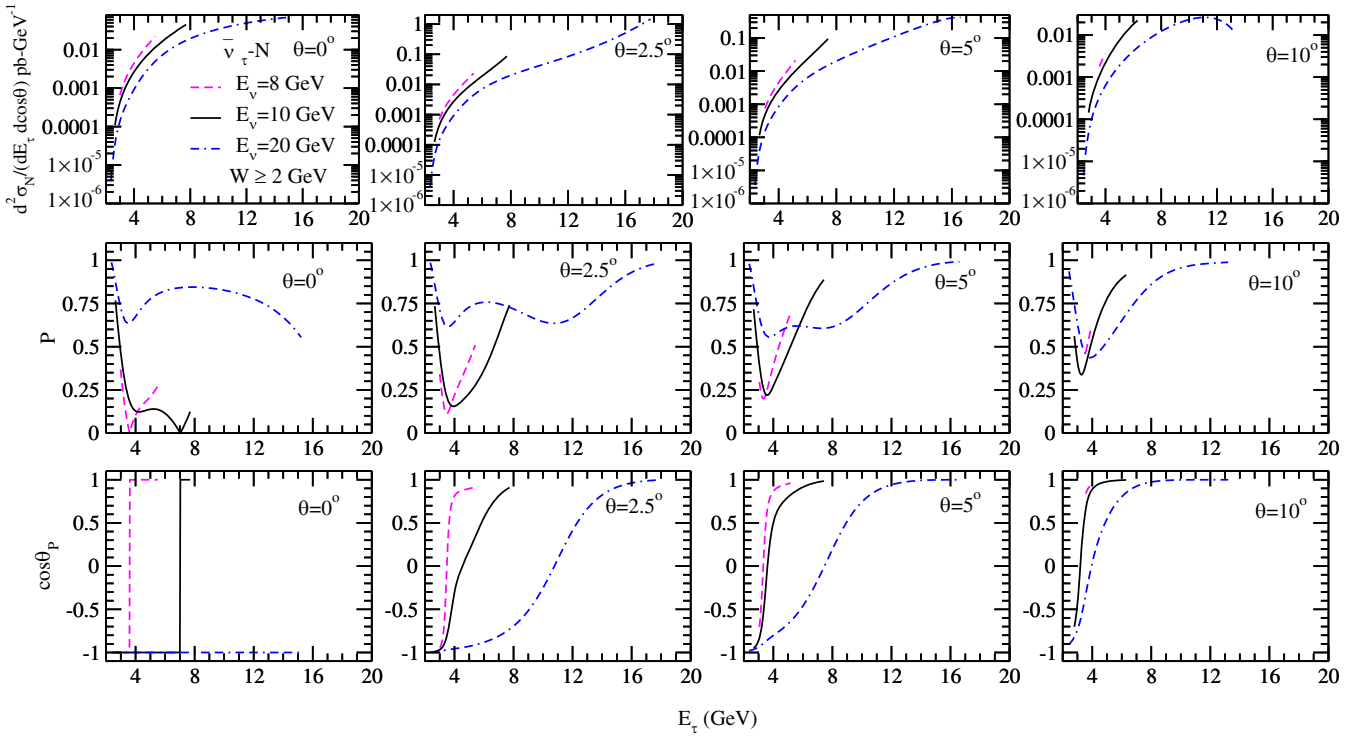

FIG. 6. *(i) Top panels:* the differential scattering cross section, *(ii) Middle panels:* the degree of polarization (P), and *(iii) Bottom panel:* the polar component of the normalized polarization vector, vs the outgoing charged lepton energy (E_τ), at the different values of incoming neutrino energy—i.e., $E_{\nu_\tau} = 8$ GeV, 10 GeV, and 20 GeV. The numerical results for $\bar{\nu}_\tau - N$ are obtained with the target mass correction effect at the next-to-leading order. These results are obtained for $W \geq 2$ GeV cuts on the center-of-mass energy.

of polarization increases again. We find that at the forward scattering angle—i.e., $\theta = 0°$—and at $E_{\nu_\tau} = 10$ GeV, the produced τ^+ lepton possesses about 46% of the degree of polarization at $E_\tau = 3$ GeV, which reduces to 11% at $E_\tau = 6$ GeV; and at $E_\tau = 7$ GeV, τ^+ becomes almost unpolarized, as the value of P is negligible here.

(b) We also observe that with the increase in the neutrino beam energy, the degree of polarization increases—e.g., at $E_\tau = 6$ GeV and at $\theta = 2.5°$, it is found to be 36% for $E_{\nu_\tau} = 10$ GeV and 75% for $E_{\nu_\tau} = 20$ GeV.

(c) For a given value of neutrino energy and the τ-lepton energy, the degree of polarization increases with the increase in the lepton scattering angles. Quantitatively, for $E_{\nu_\tau} = 10$ GeV and $E_\tau = 6$ GeV, the degree of polarization of the τ^+ lepton is 36% at $\theta = 2.5°$, 67% at $\theta = 5°$, and 90% at $\theta = 10°$.

(3) Polar component of normalized polarization vector ($\cos\theta_P$):

(a) A comparison with Fig. 5 shows that the direction of the polarization vector for the τ^+ lepton is opposite to that for the τ^- lepton.

(b) The polarization vector of the produced τ^+ lepton has negative values of $\cos\theta_P$ (implying the τ lepton to be almost left-handed) when the charged lepton energy is low, while for the high-energy values, the direction of the polarization vector gets flipped ($\cos\theta_P \geq 0$).

(c) For a given neutrino energy E_ν and charged lepton energy E_τ, the value of $\cos\theta_P$ increases with the increase of the scattering angle. Quantitatively, at $E_\nu = 10$ GeV and $E_\tau = 5$ GeV, there is an increase of about 77% in the value of $\cos\theta_P$ at $\theta = 5°$ and ∼81% at $\theta = 10°$, as compared to the case of $\theta = 2.5°$.

We observe that qualitatively, our results for $\bar{\nu}_\tau$-induced processes also show similar behavior to the corresponding results reported by Hagiwara *et al.* [53,54], although the quantitative difference is more pronounced in this case as compared to the case of $\nu_\tau - N$ DIS discussed earlier in the text.

3. Polarization components $P_{L,T}(\tau^-)$ and $P_{L,T}(\tau^+)$

We explicitly present the results for P_L (top panel) and P_T (bottom panel) vs E_τ in Fig. 7 for various angles θ in the range of $0° \leq \theta \leq 10°$. These results are presented for both the τ^- and τ^+ leptons produced in the ν_τ- and $\bar{\nu}_\tau$-induced DIS processes, respectively, at $E_{\nu_\tau} = 10$ GeV and $E_{\nu_\tau} = 20$ GeV, in order to show the energy dependence.

(1) Longitudinal polarization component P_L:

(a) For a given lepton energy E_τ and θ, the value of $P_L(\tau^{\mp})$ increases with the neutrino energy E_{ν_τ}.

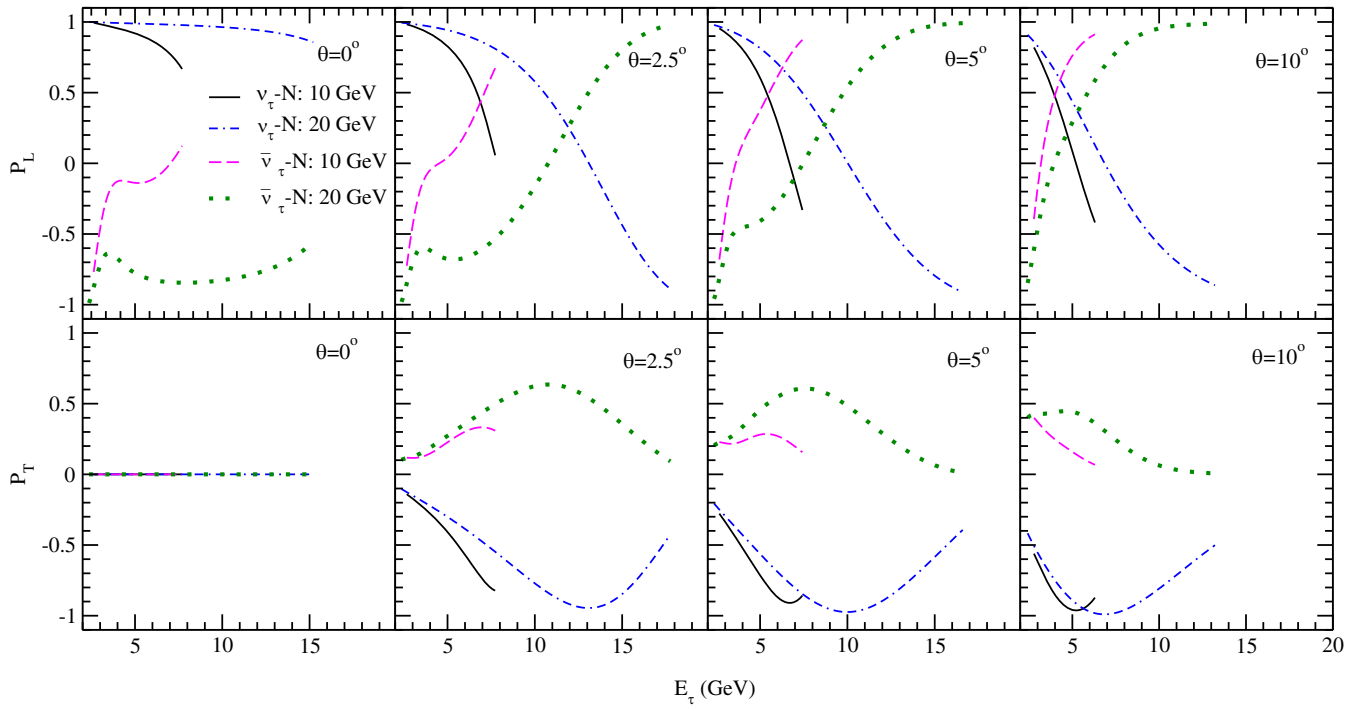

FIG. 7. *(i) Top panels:* the longitudinal component of the polarization vector (P_L) and *(iii) Bottom panels:* the transverse component of the polarization vector (P_T), vs the outgoing charged lepton energy (E_τ), at $E_{\nu_\tau} = 10$ GeV and $E_{\nu_\tau} = 20$ GeV for $\nu_\tau/\bar{\nu}_\tau - N$. The numerical results are obtained with the target mass correction effect at the next-to-leading order by considering $W \geq 2$ GeV.

(b) For a given neutrino energy, the polarization component $P_L(\tau^-)$ is large and positive (almost $+1$) at the smaller τ^--lepton energy E_τ, and it becomes negative and large (approaching -1) with the increase in E_τ. This behavior of $P_L(\tau^-)$ to approach the value of -1 at the higher lepton energies is faster at larger angles.

(c) In the case of τ^+-lepton production, the behavior of $P_L(\tau^+)$ is qualitatively similar to the behavior of τ^--lepton production, except that the sign of $P_L(\tau^+)$ for τ^+ is the opposite of the sign of $P_L(\tau^-)$ for τ^-. Quantitatively, the nature of the energy dependence with E_{ν_τ} and E_τ, and the θ dependence of $P_L(\tau^-)$ and $P_L(\tau^+)$, are different, especially at lower scattering angles θ, as shown in the figure.

(2) Transverse polarization component P_T:

In the case of the transverse polarization of the τ lepton,

(a) P_T vanishes at $\theta = 0°$. With the increase in scattering angle θ, P_T for τ^- (τ^+) increases with energy E_τ taking negative (positive) values of P_T. This increase of P_T with energy $E_{\tau^-(\tau^+)}$ continues until a critical energy $E^C_{\tau^-(\tau^+)}$, after which it decreases. The values of $E^C_{\tau^-}$ and $E^C_{\tau^+}$ depend upon the incident neutrino energy E_{ν_τ} of ν_τ and $\bar{\nu}_\tau$. In general, $E^C_{\tau^-}$ is different from $E^C_{\tau^+}$ for a given energy E_{ν_τ} for neutrinos and antineutrinos, as shown in Fig. 7 (lower panels).

(b) The angular dependence of P_T on θ for nonzero values of θ first increases and then decreases with the increase in angle θ in the region of $2.5° \leq \theta \leq 10°$, as shown in the figure.

(c) The nonvanishing values of P_T at $\theta \neq 0°$ decrease with the increase of energy E_{ν_τ}—for example, the decrease in P_T is about 20% for $E_{\nu_\tau} = 20$ GeV, as compared to $E_{\nu_\tau} = 10$ GeV at $\theta = 2.5°$ and $E_\tau = 6$ GeV.

The numerical values of P_L and P_T and their lepton energy, as well as angular dependences, are qualitatively similar to the energies and angular dependence of P_L and P_T seen in the case of quasielastic reactions [58].

B. Nuclear effects in ^{40}Ar

We have taken into account the nuclear medium effects such as the Fermi motion, the Pauli blocking, and the nucleon correlations through the nucleon spectral function, which is properly normalized to the mass number of ^{40}Ar [using Eq. (35)]. The obtained numerical results are presented in Figs. 8–11 for ν_τ- and $\bar{\nu}_\tau$-induced reactions in ^{40}Ar.

1. Neutrino-induced reactions

In Figs. 8 and 9, the results are presented for the τ^--lepton production in the charged current $\nu_\tau - {}^{40}$Ar DIS process for the projectile beam energies of $E_{\nu_\tau} = 8$ GeV and $E_{\nu_\tau} = 10$ GeV, respectively. We observe the following:

(1) Differential cross section:

(a) The effects of the nuclear medium modifications are larger in the higher region of the τ^--lepton energy and especially at the larger scattering angles. For example, when the τ-lepton energy is $E_\tau = 7$ GeV and $E_{\nu_\tau} = 10$ GeV, the differential cross section gets suppressed due to the nuclear medium effects, which is approximately a suppression of 24% at $\theta = 2.5°$, and 36% at $\theta = 5°$.

(b) The nuclear medium effects become smaller with an increase in neutrino energy, and larger with an increase in scattering angle θ. For example, when the neutrino beam energy is $E_{\nu_\tau} = 8$ GeV, the difference in the results of the differential cross sections obtained for the free nucleon target and the argon nuclear target, due to the nuclear medium modifications at $E_\tau = 3$ GeV, is found to be 28% (40%), which becomes 15% (22%) for $E_{\nu_\tau} = 10$ GeV when the lepton scattering angle is $\theta = 0°(5°)$.

(c) The allowed kinematic region for E_τ becomes more restrictive for a higher cut of the c.m. energy W. Quantitatively, when a $W \geq 1.6$ GeV cut is applied on the differential cross section obtained for $E_{\nu_\tau} = 8$ GeV at $\theta = 2.5°$, the allowed kinematic region of the τ-lepton energy is $2.9 \leq E_\tau \leq 6.2$ GeV, which reduces to $3 \leq E_\tau \leq 5.3$ GeV for a cut of $W \geq 2$ GeV.

(d) For a given τ-lepton energy E_τ, the differential cross section for the $\nu_\tau - {}^{40}$Ar scattering process reduces due to the nuclear medium effects at higher values of the cut on the c.m. energy W, unlike the scattering of ν_τ from a free nucleon target. For example, the results of the differential cross section obtained for the ^{40}Ar nuclear target at $E_\tau = 3$ GeV, with a cut of $W \geq 2$ GeV, are approximately 32% suppressed as compared to the cross section obtained with a $W \geq 1.6$ GeV cut when the neutrino beam energy is $E_\nu = 8$ GeV and $\theta = 5°$.

(2) Degree of polarization (P):

(a) There is very little change in the degree of polarization due to the nuclear medium effects at lower τ-lepton energies. For example, at $E_\tau \leq 6$ GeV, there is an increase of about 1%–2% in the results of argon as compared to the free nucleon results for all the scattering angles taken into consideration at $E_{\nu_\tau} = 10$ GeV. However, for the higher values of τ-lepton energy—say $E_\tau = 7.5$ GeV—it is found to be 9% at $\theta = 0°$ and 5% at $\theta = 2.5°$.

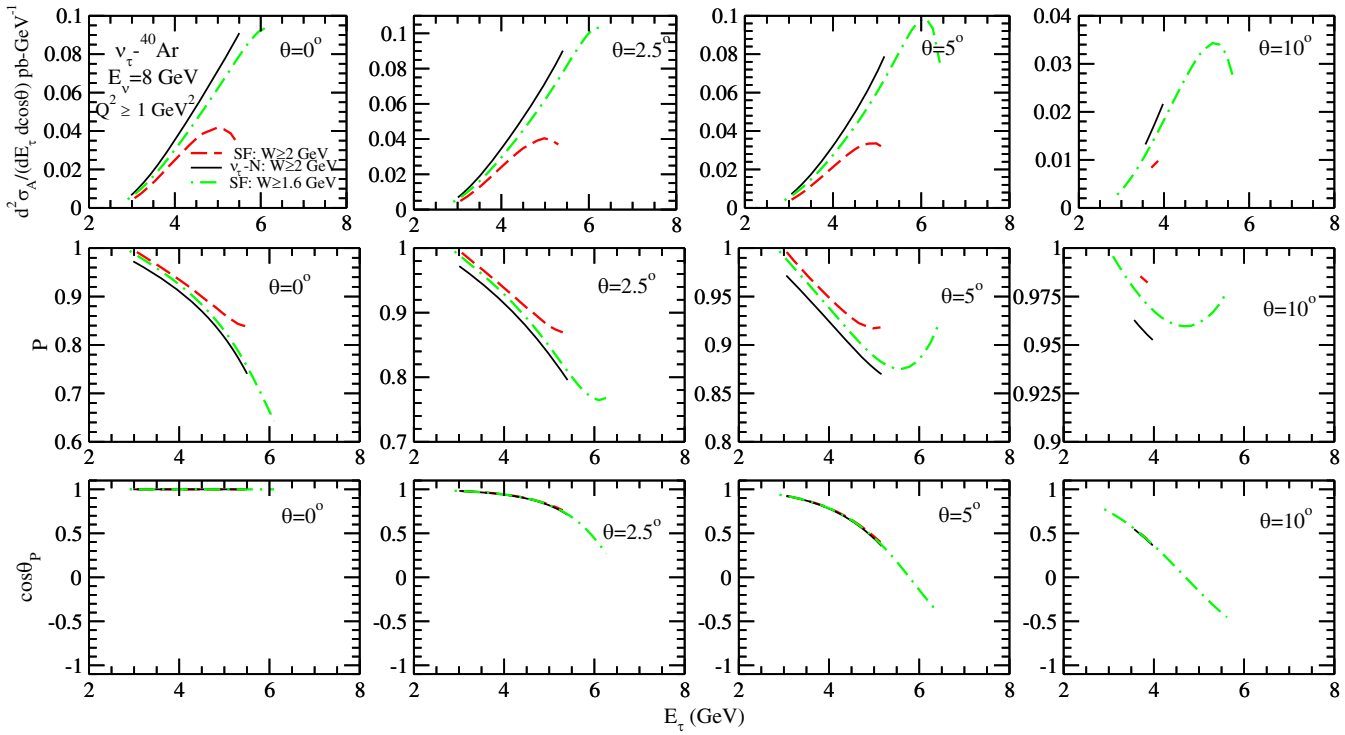

FIG. 8. *(i) Top panels:* the differential scattering cross section, *(ii) Middle panels:* the degree of polarization (P), and *(iii) Bottom panels:* the polar component of normalized polarization vector, vs the outgoing charged lepton energy (E_τ), at $E_{\nu_\tau} = 8$ GeV. The numerical results for $\nu_\tau - {}^{40}\mathrm{Ar}$ are obtained using the spectral function only (labeled as "SF"), with the target mass correction effect at the next-to-leading order found by applying a cut of $W \geq 1.6$ GeV (dash-dotted line) and $W \geq 2$ GeV (long dashed line). These results are compared with the results of the free nucleon case (solid line), obtained with a cut of 2 GeV on the c.m. energy W.

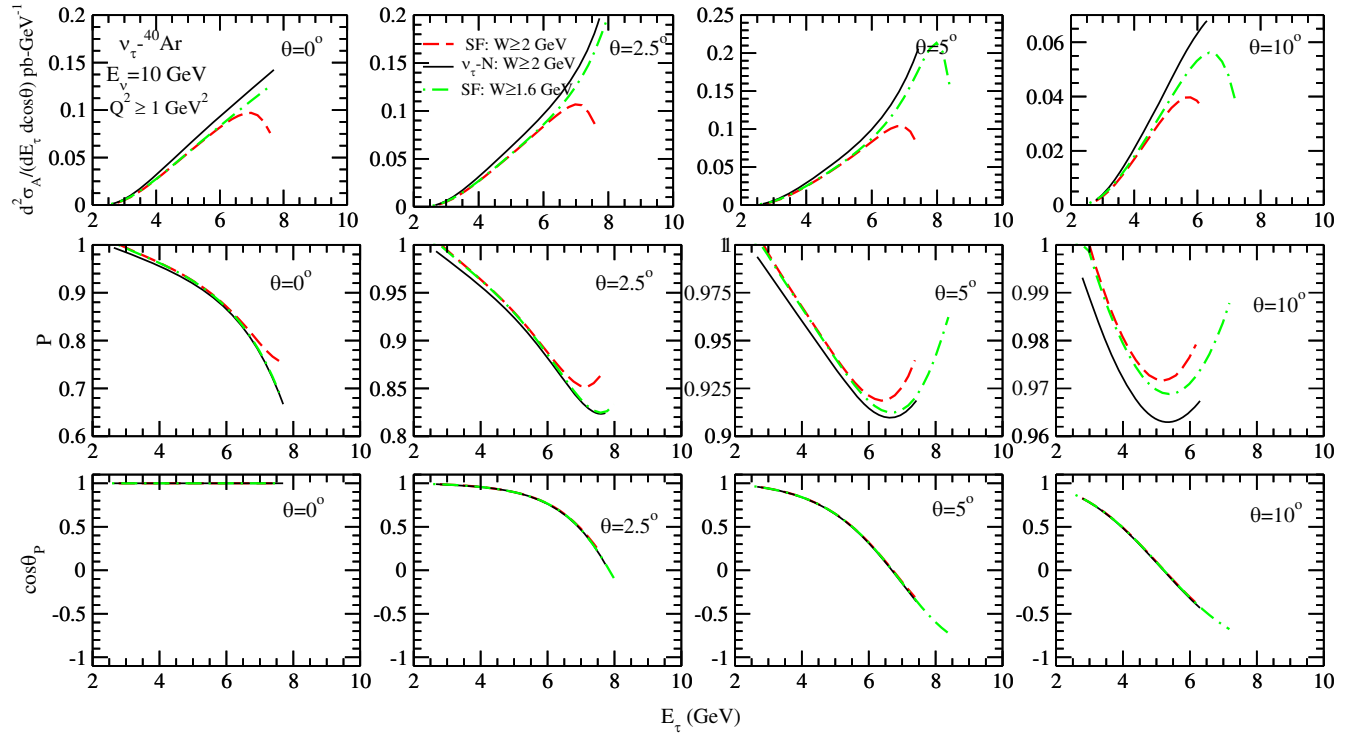

FIG. 9. *(i) Top panels:* the differential scattering cross section, *(ii) Middle panels:* the degree of polarization (P), and *(iii) Bottom panels:* the polar component of the normalized polarization vector, vs the outgoing charged lepton energy (E_τ), at $E_{\nu_\tau} = 10$ GeV for the charged current $\nu_\tau - {}^{40}\mathrm{Ar}$ DIS process. Lines in this figure have the same meaning as in Fig. 8.

(b) We observe that the effect of the nuclear medium on the degree of polarization decreases for the larger scattering angles and higher neutrino energies.

(3) Direction of polarization vector:

It is interesting to note that the effects of the nuclear medium on the direction of polarization vector are very small. The direction of the polarization vector is almost independent of the choice of kinematic constraint on the center-of-mass energy.

2. Antineutrino-induced reactions

In Figs. 10 and 11, the results are presented for the $\bar{\nu}_\tau - {}^{40}\mathrm{Ar}$ DIS process. In the case of τ^+-lepton production induced by $\bar{\nu}_\tau$, the nuclear medium effects are found to be qualitatively similar to the τ^--lepton production induced by ν_τ. However, quantitatively, there are some differences—for example:

(1) Differential cross section:

(a) We observe that for the projectile beam energy of $E_{\nu_\tau} = 8$ GeV, due to the nuclear medium effects, the differential cross section for the τ^+-lepton production is reduced by about 34% at $\theta = 2.5°$ and 45% at $\theta = 5°$, when E_τ is fixed at 3 GeV.

(b) At higher values of E_τ, the nuclear medium effects become more pronounced—for example, at $E_\tau = 5$ GeV, the reduction in the differential cross section for argon is found to be 47% at $\theta = 2.5°$ and 55% at $\theta = 5°$, as compared to the case of free nucleons.

(c) With the increase in E_{ν_τ}, the nuclear medium effects get reduced similarly to the case of τ^--lepton production. Quantitatively, for $E_{\nu_\tau} =$ 10 GeV, there is a reduction of about 30% at $\theta = 0°$ and 41% at $\theta = 5°$, as compared to the case of $E_{\nu_\tau} = 8$ GeV when E_τ is fixed at 5 GeV.

(d) The nuclear medium effects for τ^+-lepton production are found to be quantitatively different than the case of τ^--lepton production. For example, there is a difference of about 4%–5% at $E_\tau = 3$ GeV and approximately 3%–4% at $E_\tau = 5$ GeV in the range of $0° \le \theta \le 10°$.

(e) The impact of the c.m. energy cut on the τ^+-lepton production cross section is found to be qualitatively similar to the case of τ^--lepton production, as stated in Sec. III B 1 under item [I] (iv).

(2) Degree of polarization (P):

(a) The τ^+ lepton has a comparatively lower degree of polarization at the moderate values of E_τ; however, at the extreme ends, it has a good strength of P, except at $\theta = 0°$.

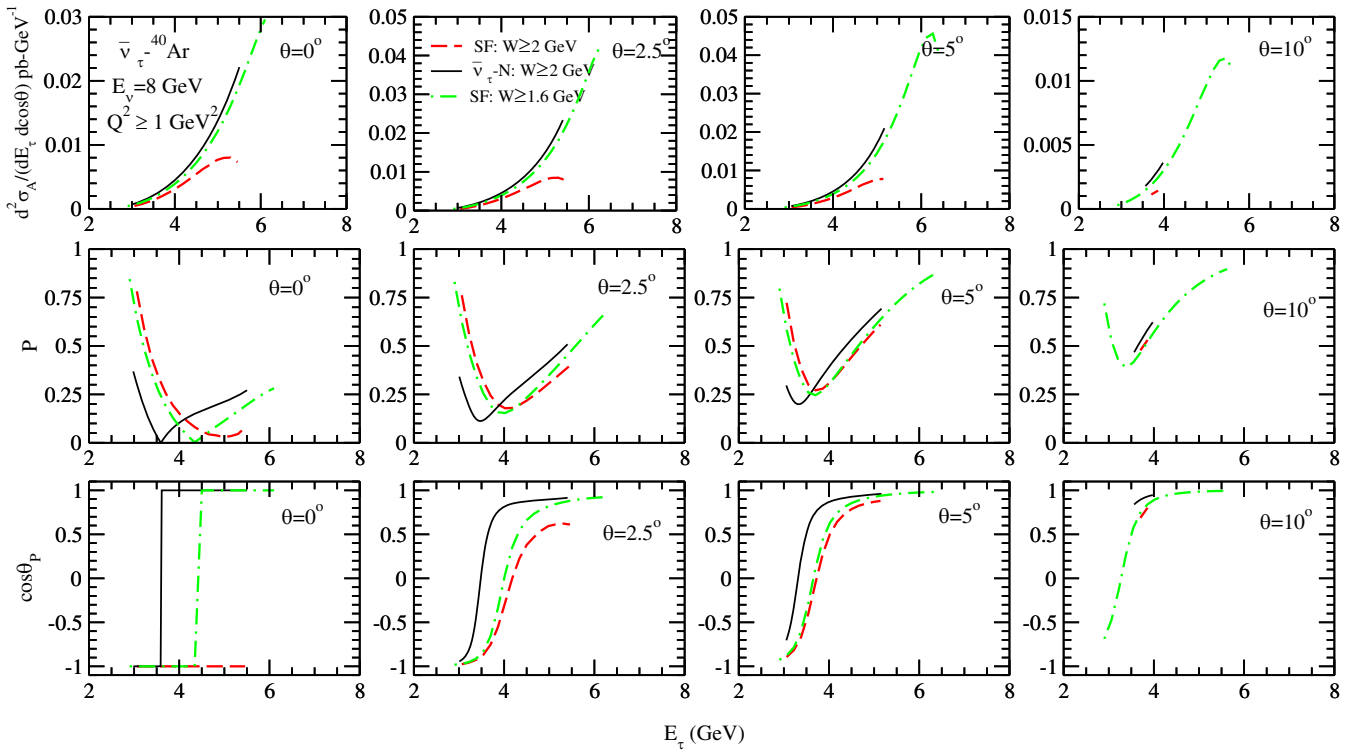

FIG. 10. *(i) Top panels:* the differential scattering cross section, *(ii) Middle panel:* the degree of polarization (P), and *(iii) Bottom panels:* the polar component of normalized polarization vector vs the outgoing charged lepton energy (E_τ) at $E_{\nu_\tau} = 8$ GeV for the charged current $\bar{\nu}_\tau - {}^{40}\mathrm{Ar}$ DIS process. Lines in this figure have the same meaning as in Fig. 8.

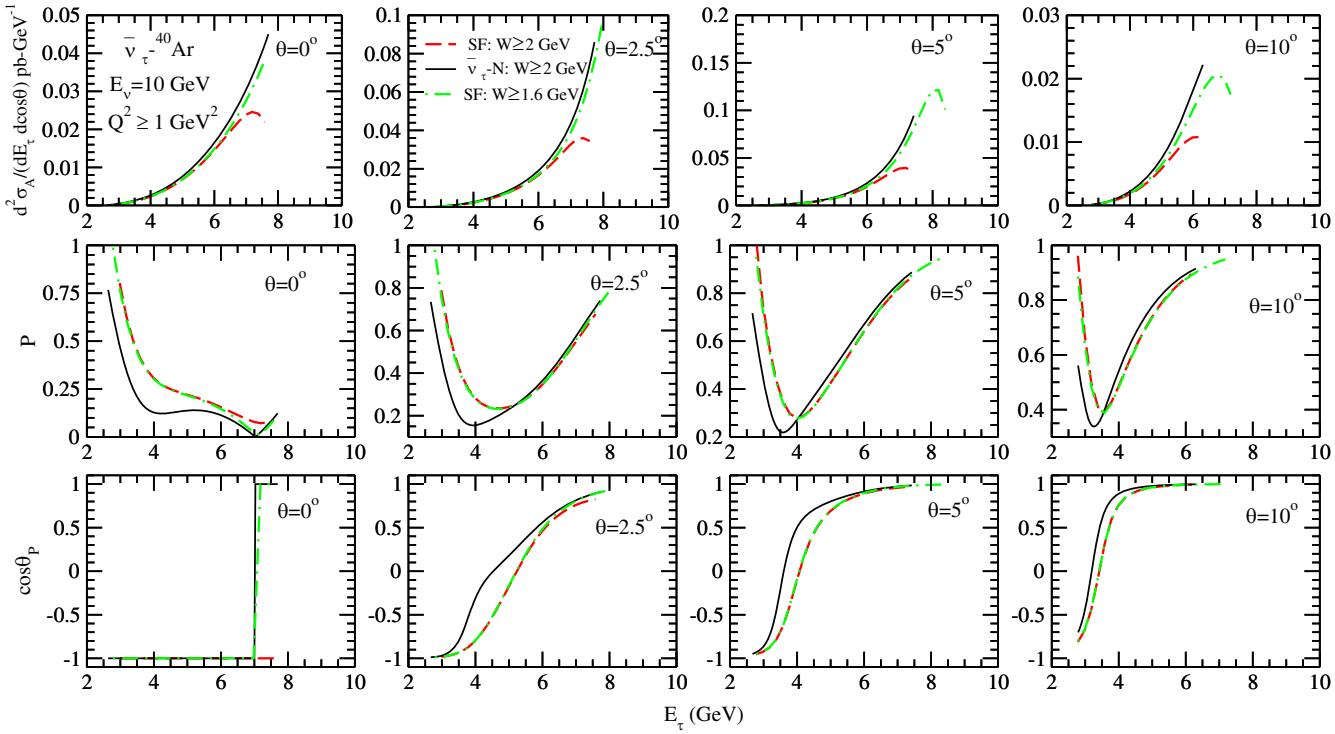

FIG. 11. *(i) Top panels:* the differential scattering cross section, *(ii) Middle panels:* the degree of polarization (P), and *(iii) Bottom panels:* the polar component of normalized polarization vector, vs the outgoing charged lepton energy (E_τ), at $E_{\nu_\tau} = 10$ GeV for the charged current $\bar{\nu}_\tau - {}^{40}$Ar DIS process. Lines in this figure have the same meaning as in Fig. 8.

(b) In the low- and intermediate-energy regions of the τ^+ lepton, the degree of polarization increases due to the nuclear medium effects, while in the higher-energy region of E_τ, it decreases for $\theta \neq 0^\circ$. For example, at $E_{\nu_\tau} = 8$ GeV and $\theta = 2.5°$, the nuclear medium effects on the degree of polarization are approximately 55% for $E_\tau = 3$ GeV and 37% for $E_\tau = 5$ GeV.

(3) Direction of polarization vector:

(a) The value of $\cos\theta_P$ for the τ^+ lepton decreases due to the nuclear medium effects, except at $\theta = 0°$. For example, on comparing the results obtained with a cut of $W \geq 2$ GeV at $\theta = 0°$, we observe that the value of $\cos\theta_P$ remains -1 in the entire range of E_τ when $\bar{\nu}_\tau$ interacts with a nucleon bound inside the argon nuclear target; however, in the case of a free nucleon target, $\cos\theta_P$ is -1 up to a certain value of E_τ, after which the direction of polarization vector gets flipped and it becomes $+1$.

(b) It is also noticeable that at $\theta = 0°$, the results obtained for ^{40}Ar with a lower cut on W—i.e., 1.6 GeV—also show similar behavior to that observed in the case of a free nucleon target.

(c) The nuclear medium effects on $\cos\theta_P$ for τ^+-lepton production are found to be larger than observed in the case of τ^--lepton production. Quantitatively, for $E_\nu = 10$ GeV and $\theta = 2.5°$, the nuclear medium effects are approximately 60% larger for the τ^+ lepton as compared to the τ^- lepton at $E_\tau = 4$ GeV, and ∼20% larger at $E_\tau = 6$ GeV.

To conclude, in this work we have studied $\tau^\pm$-lepton polarization in the presence of nuclear medium effects for the charged current $\nu_\tau/\bar{\nu}_\tau - {}^{40}$Ar deep inelastic scattering. This study may be helpful in reducing the existing systematic uncertainties in the determination of the (anti)neutrino-nucleon and (anti)neutrino-nucleus scattering cross sections. Moreover, this work may be useful for ongoing and upcoming experiments such as FASERν, SND@LHC, DUNE, and the IceCube upgrade in estimating the background events in the $\nu_\mu \to \nu_e$ appearance mode, as well as in performing the more precise measurements of the scattering cross sections. We plan to study the decay distributions of the polarized charged τ leptons and will report them in future communications.

ACKNOWLEDGMENTS

F. Z. is thankful to the Council of Scientific & Industrial Research, Government of India, for providing a Senior Research Associateship (SRA) under the Scientist's Pool Scheme, File No. 13(9240-A)2023-POOL, and to the

Department of Physics, Aligarh Muslim University, Aligarh for providing the necessary facilities to pursue this research work. M. S. A. is thankful to the Department of Science and Technology (DST), Government of India, for providing financial assistance under Grant No. SR/MF/PS-01/2016-AMU/G.

[1] R. Mammen Abraham, J. Alvarez-Muñiz, C. A. Argüelles, A. Ariga, T. Ariga, A. Aurisano, D. Autiero, M. Bishai, N. Bostan, M. Bustamante *et al.*, J. Phys. G **49**, 110501 (2022).
[2] A. Pich, Eur. Phys. J. Plus **136**, 1117 (2021).
[3] M. L. Perl, G. S. Abrams, A. Boyarski, M. Breidenbach, D. Briggs, F. Bulos, W. Chinowsky, J. T. Dakin, G. J. Feldman, C. E. Friedberg *et al.*, Phys. Rev. Lett. **35**, 1489 (1975).
[4] K. Kodama *et al.* (DONUT Collaboration), Phys. Lett. B **504**, 218 (2001).
[5] N. Agafonova *et al.* (OPERA Collaboration), Phys. Rev. Lett. **115**, 121802 (2015).
[6] K. Kodama *et al.* (DONUT Collaboration), Phys. Rev. D **78**, 052002 (2008).
[7] N. Agafonova *et al.* (OPERA Collaboration), Phys. Rev. Lett. **120**, 211801 (2018); **121**, 139901(E) (2018).
[8] P. Astier *et al.* (NOMAD Collaboration), Nucl. Phys. **B611**, 3 (2001).
[9] Z. Li *et al.* (Super-Kamiokande Collaboration), Phys. Rev. D **98**, 052006 (2018).
[10] M. G. Aartsen *et al.* (IceCube Collaboration), Phys. Rev. D **99**, 032007 (2019).
[11] R. Abbasi *et al.* (IceCube Collaboration), Eur. Phys. J. C **82**, 1031 (2022).
[12] S. Aoki *et al.* (DsTau Collaboration), J. High Energy Phys. 01 (2020) 033.
[13] M. Anelli *et al.* (SHiP Collaboration), arXiv:1504.04956.
[14] H. Abreu *et al.* (FASER Collaboration), Eur. Phys. J. C **80**, 61 (2020).
[15] H. Abreu *et al.* (FASER Collaboration), arXiv:2001.03073.
[16] K. Jodłowski and S. Trojanowski, J. High Energy Phys. 05 (2021) 191.
[17] H. Abreu *et al.* (FASER Collaboration), Phys. Rev. Lett. **131**, 031801 (2023).
[18] C. Ahdida *et al.* (SHiP Collaboration), arXiv:2002.08722.
[19] G. Acampora *et al.* (SND@LHC Collaboration), arXiv:2210.02784.
[20] A. De Gouvêa, K. J. Kelly, G. V. Stenico, and P. Pasquini, Phys. Rev. D **100**, 016004 (2019).
[21] B. Abi *et al.* (DUNE Collaboration), arXiv:2002.03005.
[22] A. Ishihara (IceCube Collaboration), Proc. Sci. ICRC2019 (**2021**) 1031.
[23] M. G. Aartsen *et al.* (IceCube-Gen2 Collaboration), J. Phys. G **48**, 060501 (2021).
[24] K. Abe *et al.* (Hyper-Kamiokande Collaboration), arXiv:1805.04163.
[25] J. Yu, Proc. Sci. ICHEP2018 (**2019**) 703.
[26] S. Weinberg, Phys. Rev. Lett. **19**, 1264 (1967).
[27] A. Salam, Conf. Proc. C **680519**, 367 (1968).
[28] S. L. Glashow, J. Iliopoulos, and L. Maiani, Phys. Rev. D **2**, 1285 (1970).
[29] R. Aaij *et al.* (LHCb Collaboration), Phys. Rev. Lett. **113**, 151601 (2014).
[30] R. Aaij *et al.* (LHCb Collaboration), Phys. Rev. Lett. **115**, 111803 (2015); **115**, 159901(E) (2015).
[31] R. Aaij *et al.* (LHCb Collaboration), Phys. Rev. D **108**, 012018 (2023).
[32] B. Aubert *et al.* (*BABAR* Collaboration), Phys. Rev. Lett. **100**, 021801 (2008).
[33] J. P. Lees *et al.* (*BABAR* Collaboration), Phys. Rev. Lett. **109**, 101802 (2012).
[34] A. Matyja *et al.* (Belle Collaboration), Phys. Rev. Lett. **99**, 191807 (2007).
[35] I. Adachi *et al.* (Belle Collaboration), arXiv:0910.4301.
[36] A. Bozek *et al.* (Belle Collaboration), Phys. Rev. D **82**, 072005 (2010).
[37] E. Kou *et al.* (Belle-II Collaboration), Prog. Theor. Exp. Phys. **2019**, 123C01 (2019); **2020**, 029201(E) (2020).
[38] J. Portoles, Rev. Mex. Fis. Suppl. **3**, 020715 (2022).
[39] P. Lipari, M. Lusignoli, and F. Sartogo, Phys. Rev. Lett. **74**, 4384 (1995).
[40] J. Conrad, A. de Gouvea, S. Shalgar, and J. Spitz, Phys. Rev. D **82**, 093012 (2010).
[41] V. Ansari, M. Sajjad Athar, H. Haider, S. K. Singh, and F. Zaidi, Phys. Rev. D **102**, 113007 (2020).
[42] F. Zaidi, V. Ansari, M. S. Athar, H. Haider, I. R. Simo, and S. K. Singh, Phys. Rev. D **105**, 033010 (2022).
[43] M. G. Aartsen *et al.* (IceCube Collaboration), Phys. Rev. D **93**, 022001 (2016).
[44] D. Van Eijk, SciPost Phys. Proc. **1**, 030 (2019).
[45] N. Song, S. W. Li, C. A. Argüelles, M. Bustamante, and A. C. Vincent, J. Cosmol. Astropart. Phys. 04 (2021) 054.
[46] J. Tena-Vidal *et al.* (GENIE Collaboration), Phys. Rev. D **104**, 072009 (2021).
[47] C. Andreopoulos, C. Barry, S. Dytman, H. Gallagher, T. Golan, R. Hatcher, G. Perdue, and J. Yarba, arXiv:1510.05494.
[48] T. Leitner, L. Alvarez-Ruso, and U. Mosel, Phys. Rev. C **73**, 065502 (2006).
[49] O. Buss, T. Gaitanos, K. Gallmeister, H. van Hees, M. Kaskulov, O. Lalakulich, A. B. Larionov, T. Leitner, J. Weil, and U. Mosel, Phys. Rep. **512**, 1 (2012).
[50] T. Golan, J. T. Sobczyk, and J. Zmuda, Nucl. Phys. B, Proc. Suppl. **229–232**, 499 (2012).
[51] Y. Hayato and L. Pickering, Eur. Phys. J. Special Topics **230**, 4469 (2021).
[52] J. Isaacson, S. Höche, F. Siegert, and S. Wang, arXiv:2303.08104.

[53] K. Hagiwara, K. Mawatari, and H. Yokoya, Nucl. Phys. B **668**, 364 (2003); **701**, 405(E) (2004).
[54] K. Hagiwara, K. Mawatari, and H. Yokoya, Nucl. Phys. B, Proc. Suppl. **139**, 140 (2005).
[55] M. Aoki, K. Hagiwara, K. Mawatari, and H. Yokoya, Nucl. Phys. B **727**, 163 (2005).
[56] K. S. Kuzmin, V. V. Lyubushkin, and V. A. Naumov, Mod. Phys. Lett. A **19**, 2815 (2004).
[57] K. S. Kuzmin, V. V. Lyubushkin, and V. A. Naumov, Mod. Phys. Lett. A **19**, 2919 (2004).
[58] K. S. Kuzmin, V. V. Lyubushkin, and V. A. Naumov, Nucl. Phys. B, Proc. Suppl. **139**, 154 (2005).
[59] K. Kurek, Nucl. Phys. B, Proc. Suppl. **139**, 146 (2005).
[60] A. Fatima, M. Sajjad Athar, and S. K. Singh, Phys. Rev. D **102**, 113009 (2020).
[61] A. Fatima, M. S. Athar, and S. K. Singh, Phys. Rev. D **105**, 073004 (2022).
[62] M. Sajjad Athar, A. Fatima, and S. K. Singh, Prog. Part. Nucl. Phys. **129**, 104019 (2023).
[63] K. M. Graczyk and B. E. Kowal, Phys. Rev. D **97**, 013001 (2018).
[64] C. H. Albright and C. Jarlskog, Nucl. Phys. B **84**, 467 (1975).
[65] K. M. Graczyk, Nucl. Phys. B, Proc. Suppl. **139**, 150 (2005).
[66] C. Bourrely, J. Soffer, and O. V. Teryaev, Phys. Rev. D **69**, 114019 (2004).
[67] A. D. Martin, R. G. Roberts, W. J. Stirling, and R. S. Thorne, Eur. Phys. J. C **23**, 73 (2002).
[68] M. Glück, E. Reya, and A. Vogt, Eur. Phys. J. C **5**, 461 (1998).
[69] A. Bodek and U. K. Yang, Nucl. Phys. B, Proc. Suppl. **112**, 70 (2002).
[70] J. Mousseau *et al.* (MINERvA Collaboration), Phys. Rev. D **93**, 071101 (2016).
[71] J. J. Aubert *et al.* (European Muon Collaboration), Phys. Lett. B **123**, 275 (1983).
[72] B. G. Tice *et al.* (MINERvA Collaboration), Phys. Rev. Lett. **112**, 231801 (2014).
[73] K. M. Graczyk, Nucl. Phys. A **748**, 313 (2005).
[74] M. Valverde, J. E. Amaro, J. Nieves, and C. Maieron, Phys. Lett. B **642**, 218 (2006).
[75] J. Lagoda, D. Kielczewska, M. Posiadala, R. Sulej, K. Zaremba, T. Kozlowski, K. Kurek, P. Mijakowski, P. Przewlocki, E. Rondio *et al.*, Acta Phys. Pol. B **38**, 2083 (2007).
[76] J. E. Amaro, C. Maieron, M. Valverde, J. Nieves, M. B. Barbaro, J. A. Caballero, T. W. Donnelly, and J. M. Udias, AIP Conf. Proc. **1189**, 24 (2009).
[77] J. E. Sobczyk, N. Rocco, and J. Nieves, Phys. Rev. C **100**, 035501 (2019).
[78] E. Hernández, J. Nieves, F. Sánchez, and J. E. Sobczyk, Phys. Lett. B **829**, 137046 (2022).
[79] F. Zaidi, H. Haider, M. Sajjad Athar, S. K. Singh, and I. Ruiz Simo, Phys. Rev. D **101**, 033001 (2020).
[80] V. Ansari, M. S. Athar, H. Haider, I. R. Simo, S. K. Singh, and F. Zaidi, Eur. Phys. J. Special Topics **230**, 4433 (2021).
[81] M. Sajjad Athar, S. K. Singh, and F. Zaidi, Phys. Rev. D **105**, 093002 (2022).
[82] F. Zaidi, V. Ansari, H. Haider, M. Sajjad Athar, and S. K. Singh, Springer Proc. Phys. **277**, 541 (2022).
[83] M. Sajjad Athar and J. G. Morfín, J. Phys. G **48**, 034001 (2021).
[84] S. Kretzer and M. H. Reno, Phys. Rev. D **66**, 113007 (2002).
[85] S. Kretzer and M. H. Reno, Phys. Rev. D **69**, 034002 (2004).
[86] P. Fernandez de Cordoba and E. Oset, Phys. Rev. C **46**, 1697 (1992).
[87] E. Marco, E. Oset, and P. Fernández de Córdoba, Nucl. Phys. A **611**, 484 (1996).
[88] H. Haider, F. Zaidi, M. Sajjad Athar, S. K. Singh, and I. Ruiz Simo, Nucl. Phys. A **955**, 58 (2016).
[89] C. G. Callan, Jr. and D. J. Gross, Phys. Rev. Lett. **22**, 156 (1969).
[90] L. A. Harland-Lang, A. D. Martin, P. Motylinski, and R. S. Thorne, Eur. Phys. J. C **75**, 204 (2015).
[91] C. W. De Jager, H. De Vries, and C. De Vries, At. Data Nucl. Data Tables **14**, 479 (1974); **16**, 580(E) (1975).
[92] H. De Vries, C. W. De Jager, and C. De Vries, At. Data Nucl. Data Tables **36**, 495 (1987).
[93] H. Haider, F. Zaidi, M. Sajjad Athar, S. K. Singh, and I. Ruiz Simo, Nucl. Phys. A **943**, 58 (2015).
[94] H. Haider, I. Ruiz Simo, and M. Sajjad Athar, Phys. Rev. C **85**, 055201 (2012).
[95] F. Zaidi, H. Haider, M. Sajjad Athar, S. K. Singh, and I. Ruiz Simo, Phys. Rev. D **99**, 093011 (2019).